Robust Hybrid Linear Modeling and its Applications

A DISSERTATION
SUBMITTED TO THE FACULTY OF THE GRADUATE SCHOOL
OF THE UNIVERSITY OF MINNESOTA
BY

Yi Wang

IN PARTIAL FULFILLMENT OF THE REQUIREMENTS
FOR THE DEGREE OF
Doctor of Philosophy

Gilad Lerman

July, 2012

Acknowledgements

Foremost, I would like to express my sincere gratitude to my advisor Prof. Gilad Lerman for the continuous support of my Ph.D study and research, for his patience, motivation, enthusiasm, and immense knowledge. His guidance helped me in all the time of research and writing of this thesis. I could not have imagined having a better advisor and mentor for my Ph.D study. I also thank my collaborator, Dr. Arthur Szlam, for his inspiring ideas and guidance.

Besides my advisor, I would like to thank the rest of my thesis committee: Prof. Fadil Santosa, Prof. Andrew Odlyzko, and Prof. Snigdhansu Chatterjee, for their encouragement, insightful comments and hard questions.

My sincere thanks also go to Dr. Fatih Porikli and Dr. Hao Vu, for offering me the summer internship opportunities in their groups and leading me working on diverse exciting projects.

I thank my classmates in the same research group: Guangliang Chen, Teng Zhang and Bryan Poling for the stimulating and enlightening discussions. Also I thank my great friends from the Club of Amazing Mathematics & Engineering Ladies (CAMEL) at the UMN, including Xingjie Li, Hao Zhu, Huiqiong Deng, Xiaoqing He, Hui Li, Zhihua Su and Lin Yang, for their valuable comments and suggestions.

Last but not the least, I would like to thank my parents Lijun Shao and Yehong Wang, for giving birth to me at the first place and supporting me spiritually throughout my life.

Abstract

Hybrid Linear Modeling (HLM) uses a set of affine subspaces to model data and has been widely used in computer vision. However, many segmentation algorithms need to know d and K as a priori. Therefore, determining the dimension d and the number K of subspaces is an important problem in HLM. In this manuscript, we suggest two automatic ways to empirically find d and K. One obtains local estimation of the dimension by examining the geometric structure of a neighborhood. The other finds K or both d and K by detecting the "elbow" of the least square error. We provide a partial justification of the elbow method for special cases. We also demonstrate the accuracy and speed of our methods on synthetic and real hybrid linear data.

Another challenge in HLM is to deal with highly corrupted data. We study the related problems of denoising images corrupted by impulsive noise and blind inpainting (i.e., inpainting when the deteriorated region is unknown). Our basic approach is to model the set of patches of pixels in an image as a union of low dimensional subspaces, corrupted by sparse but perhaps large magnitude noise. For this purpose, we develop a robust and iterative method for single subspace modeling and extend it to an iterative algorithm for modeling multiple subspaces. We prove convergence for both algorithms and carefully compare our methods with other recent ideas for such robust modeling. We demonstrate state of the art performance of our method for both imaging problems.

Contents

List of Tables

List of Figures

Hybrid Linear Modeling (HLM) uses a set of affine subspaces to model data and has been widely used in computer vision. However, many segmentation algorithms need to know d and K as a priori. Therefore, determining the dimension d and the number K of subspaces is an important problem in HLM. In this manuscript, we suggest two automatic ways to empirically find d and K. One obtains local estimation of the dimension by examining the geometric structure of a neighborhood. The other finds K or both d and K by detecting the "elbow" of the least square error. We provide a partial justification of the elbow method for special cases. We also demonstrate the accuracy and speed of our methods on synthetic and real hybrid linear data.

Another challenge in HLM is to deal with highly corrupted data. We study the related problems of denoising images corrupted by impulsive noise and blind inpainting (i.e., inpainting when the deteriorated region is unknown). Our basic approach is to model the set of patches of pixels in an image as a union of low dimensional subspaces, corrupted by sparse but perhaps large magnitude noise. For this purpose, we develop a robust and iterative method for single subspace modeling and extend it to an iterative algorithm for modeling multiple subspaces. We prove convergence for both algorithms and carefully compare our methods with other recent ideas for such robust modeling. We demonstrate state of the art performance of our method for both imaging problems.

Chapter 1

Introduction

1.1 Hybrid Linear Modeling

The problem of Hybrid Linear Modeling (HLM) is to model data using a union of affine subspaces and cluster it in subsets representing these subspaces. It has been widely used in many fields, such as motion segmentation, computer vision, image processing, etc (see [1] and references therein). Many HLM algorithms need the dimension d and the number K of underlying subspaces as prior knowledge to get meaningful results. Therefore determining these parameters K and d is a critical and challenging problem in this area.

Some approaches have already been suggested to determine K and possibly d in HLM. GPCA [2] embeds data to the space spanned by homogeneous polynomials and segments data in the embedded space. The number of subspaces is estimated as the minimum degree such that the embedded data matrix drops rank. Furthermore, ALC [3] uses the coding length as the criterion to merge data points, thus determines the number of clusters automatically. For estimation of K on related pairwise clustering, methods include Gap Statistic [4], X-means [5], self-tuning spectral clustering [6], etc. But these methods do not apply directly to HLM.

In this proposal, we assume all subspaces have the same dimension and explore an automatic way to find the number of subspaces by extending and modifying the idea of Gap Statistic to HLM. This method is based on the assumption that the least square error in HLM behaves as an L-curved function (see e.g. Figure 2.1, the top left) with

respect to the number of cluster K. The location of the elbow point (the tip of the L shape) indicates the empirical value for K. We also provide some partial evidence for this phenomenon. Instead of comparing the error with a reference null distribution in Gap Statistic, we use a numerical technique, second order difference (SOD) [7] in the logarithmic scale to find the elbow position.

The contributions of the first half of this manuscript are as follows.

- It suggests an automatic method to find the dimension and number of subspaces. The only assumption is that the dimensions of all subspaces are the same. The algorithm does not require the dimension, or any other parameter.
- The method can be applied to any segmentation method, because this algorithm uses only the segmentation output.
- It eliminates the use of reference null distribution in Gap Statistic by using SOD and also efficiently implements this idea. And this modification makes the method faster and more stable.
- Some partial justification for the elbow phenomenon in special cases is provided.

1.2 Robust Locally Linear Analysis

We also consider the problem of denoising images corrupted with impulsive noise, and the problem of blind inpainting where the image has been "scratched". In both of these settings, some percentage of the pixels of the image have been grossly corrupted and the locations and the values of the corrupted pixels are unknown. In the former, it is assumed that the corruptions are unstructured, whereas the latter has geometrically structured corruptions (e.g., lying along curves). We take advantage of some recent progress in sparse coding, dictionary design, and geometric data modeling in order to develop a method with state-of-the-art performance on these two problems. There are some recent work dealing with these problems with wavelet frame and total variation [8, 9].

Sparse coding and dictionary design have been shown to be effective at denoising images corrupted with Gaussian noise as well as at standard inpainting with corruptions

in known locations [10]. The basic approach is to fix a width $\sqrt{m}$, and extract all the $\sqrt{m} \times \sqrt{m}$ patches from the image, forming an $m \times n$ matrix $\mathbf{X}$, where n is the number of patches. Then $\mathbf{X}$ is decomposed into

$$\mathbf{DA} \simeq \mathbf{X},$$

where $\mathbf{D}$ is an $m \times k$ dictionary matrix, and $\mathbf{A}$ is the matrix of coefficients; $\mathbf{A}$ is either constrained to be sparse or encouraged to be sparse via a regularization term. One can learn both $\mathbf{A}$ and $\mathbf{D}$ and create a model for $\mathbf{X}$ that can be used for both denoising and inpainting.

Yu et al. [11] suggested a structured sparsity constraint. That is, they require $\mathbf{A}$ to have a block structure with a prespecified number of blocks; each block corresponds to a fixed set of columns of $\mathbf{D}$. They learn this structure by partitioning $\mathbf{X}$ into clusters associated to subdictionaries of $\mathbf{D}$ via a variant of the K-subspaces algorithm [12, 13, 14, 15]. Given parameters r and K, this algorithm attempts to find K r-dimensional subspaces, represented by $m \times q$ (where $q < m$) orthogonal matrices $\mathbf{D}_1, ..., \mathbf{D}_K$ (i.e., matrices with orthonormal columns), which minimize

$$\sum_{j=1}^{N} \min_{1 \le i \le K} \|\mathbf{x}_j - \mathbf{D}_i \mathbf{D}_i^T \mathbf{x}_j\|^2. \tag{1.1}$$

Finding $\mathbf{D} = [\mathbf{D}_1, ...\mathbf{D}_K]$ can be thought of as a block structured dictionary learning problem, or as finding the best secant subspaces to the given data set. The block structure benefits the denoising by making the coding more stable [11].

The optimization for the K-subspaces model can be done via Lloyd iteration: holding the clusters fixed, find the best $\mathbf{D}$, and then update the clusters. With the clustering fixed, the problem reduces to finding the best rank r approximation to the columns in $\mathbf{X}$ associated to the cluster. In the case of Gaussian noise, "best" is usually chosen to be measured by Frobenius norm, in which case the solution is given via SVD.

In this manuscript we adapt the approach of [11] to images corrupted by impulsive noise (and perhaps with additional Gaussian noise) as well as to blind inpainting. In this framework, finding $\mathbf{D} = [\mathbf{D}_1, ...\mathbf{D}_K]$ with the clusters fixed requires a different tool than the SVD. In particular, we will need a "robust" low rank method, which allows large corruptions of a controlled percentage of the corresponding matrix, in order to

obtain a robust sparse coding method. Recently, there has been a large interest in developing robust low rank models for matrices corrupted this way [16, 17, 18]. Our goal is to locally use such a low rank model in a framework like K-subspaces for image denoising and blind inpainting. However, we will find that these recent methods of low rank modeling are not well suited to this task, and will use instead a greedy and fast method for the updates of the dictionary $\mathbf{D}$.

The major contributions of the second part of this manuscript are as follows:

1. We describe an alternating least squares (ALS) algorithm for robust recovery of low rank matrices and compare it to other low-rank modeling algorithms (for the same corruption model).

2. We introduce local versions of the ALS (and other low-rank modeling algorithms) for block structured dictionary learning (or equivalently locally linear modeling) in the presence of large and sparse corruptions.

3. We prove that under some mild conditions the ALS algorithm and its local version (the K-ALS algorithm) converge to a fixed point with probability 1.

4. We show how the local methods can be used for image denoising with impulsive noise and blind inpainting. In addition to five common images, we use a database of 100 images to demonstrate the state of the art performance by our method.

Chapter 2

Hybrid Linear Modeling

2.1 Background

In this section, we introduce the background of HLM and elbow heuristic of L-curved function.

2.1.1 Hybrid Linear Modeling

There are various strategies to solve the HLM problem [12, 19, 20, 21, 13, 14, 22, 23, 15, 2, 24, 25, 1, 3, 26, 27, 28, 29]. We will choose the Local Best-fit Flats (LBF) [29] for HLM later in our method. LBF is a very simple geometric method based on selecting a set of local best fit flats that minimize a global l_1 error measure. Our preference to LBF is due to its tested accuracy on artificial and applied data, speed (to our best knowledge, it is the fastest one) and ability to handle relative large K and d.

2.1.2 Elbow Method

Most HLM problems suffer from a trade-off between the complexity and the quality of the model to the given data. In practice, the plot of the least square error versus the number of subspaces resembles the letter "L". The statistical folklore has it that the location of the elbow in this plot indicates the appropriate model with fair complexity which fits the data well enough.

In the problem of determining the number of clusters, we define the sum of least

square errors of the data points to the flats they belong. And this error would decrease monotonically as the number of clusters K increases. However, after some number K_{opt}, the decrease would flatten remarkably. Then K_{opt} would be the appropriate number of clusters. See [4, 30] for more information.

2.2 Automatic Determination of the Dimension and the Number of Subspaces

We assume the dimensions of all the subspaces are the same and suggest two methods to find the appropriate dimension and the number of subspaces in this section.

2.2.1 A Local Estimation of the Dimension

We propose a local estimation of the dimension (LED) for the data. For a fixed point with a fixed neighborhood size m, we estimate its empirical dimension as follows. We form the centered matrix of data points in this neighborhood (subtracting the fixed point) and compute its singular values $\sigma_1 \geq \sigma_2 \geq \cdots \geq \sigma_m$. The empirical dimension d is the smallest number such that $\sigma_d > 2\sigma_{d+1}$. If no such number exists or $d > D$, we let $d = D$.

For a fixed point, we start with $m = 20$, and while $d = D$ and $m \leq 70$, we increase m and update the value of d. We run this estimation at each point and choose the empirical dimension for the whole data by majority.

2.2.2 Number of Clusters via the Elbow Method

Let d and D be integers such that $0 \leq d < D$. We have $X = \{\mathbf{x}_1, \mathbf{x}_2, \ldots, \mathbf{x}_N\} \subset \mathbb{R}^D$ and assume that X is segmented to K clusters $C_1, \ldots, C_K$ and $K \leq K_{max}$. Then the within cluster sum square errors $\{W_K\}$, $K = 1, \ldots, K_{max}$ is defined as follows:

$$W_K = \sum_{j=1}^{K} \sum_{\mathbf{x} \in C_j} dist^2(\mathbf{x}, F_j), \tag{2.1}$$

where K_{max} is the possible max number of clusters, F_j is the Orthogonal Least Squares(OLS) $d-$ flat approximating C_K (obtained by Principal Component Analysis(PCA)), and $dist(\mathbf{x}, F_j)$ denotes the orthogonal distance from $\mathbf{x}$ to F_j.

As K increases, W_K decreases. A classical method for determining the number of clusters is to find the "elbow", or the K past which adding more clusters does not significantly decrease the error. We search for the elbow by finding the maximum of the Second Order Difference (SOD) of the logarithm of W_K [7]:

$$\mathrm{SOD}(\ln W_K) = \ln W_{K-1} + \ln W_{K+1} - 2\ln W_K, \tag{2.2}$$

So that the optimal K is found by:

$$K_{\mathrm{SOD}} = \arg\max_K \mathrm{SOD}(\ln W_K). \tag{2.3}$$

where $K = 2, \ldots, K_{max}$.

2.2.3 Simultaneous Estimation of Dimension and Number of Clusters via Elbow Method

In this section, we suggest an application of the elbow method for estimating both the dimension and the number of clusters assuming the same dimension for all clusters. We first fix the dimension d and find the optimal number of clusters K_d by the algorithm of the previous section. Then we reapply SOD on $\{W_{K_d}\}, d = 0, 1, \ldots, d_{max}$ to find an optimal dimension d_{SOD} past which adding complexity to the model cannot significantly reduce the error. The output of this method, which we refer as SOD2, is both d_{SOD} and $K_{d_{\mathrm{SOD}}}$. In practice, we let $W_D = 0$ and add 1 to the least square errors (as in equation 2.2) in order to possibly find $d_{\mathrm{SOD}} = D - 1$.

2.3 Algorithm

In this section, we state algorithms 1 and 2 which finds the appropriate number of clusters K or both K and dimension d. In the algorithms, we use the LBF [29] (or spectral clustering when $d = 0$) as the segmentation method. Any other algorithm which can find hybrid linear clusters for given K and d is applicable.

2.4 Theoretical Computation

To examine further our SOD method, we do the theoretical computation for some continuous cases. And the results well support our algorithms. In the examples, we

Algorithm 1 The Second Order Difference with equal and known dimension(SOD)

Require: $X = \{\mathbf{x}_1, \mathbf{x}_2, \ldots, \mathbf{x}_N\} \subset \mathbb{R}^D$:data, d:dimensions, K_{max}:the estimated largest number of clusters.
Ensure: K_{SOD} disjoint cluster $C_1, \ldots, C_{K_{\mathrm{SOD}}}$.
Steps:
for $K = 2, \ldots, K_{max}$ **do**

Apply $LBF(d, K)$ on X.
Record the labels in $Labels\{K\}$.
Calculate W_K by equation 2.1.
end for

Calculate $SOD(\ln W)_K$ by equation 2.2.
Find K_{SOD} by equation 2.3.
Return the labels $Labels\{K_{\mathrm{SOD}}\}$ and K_{SOD}.

assume $d = 1$ and look for optimal K. We also assume that each underlying linear subspace has the conic noise with angle θ around it and we obtain the ideal segmentation.

For a linear subspace $L \subseteq H$ and an angle α such that $0 \leq \alpha \leq \pi/2$, we define the *cone*, $C_{one}(\alpha, L)$, centered at the origin on L in the following way[31]:

$$C_{one}(\alpha, L) := \{u \in H : dist(u, L) \leq ||u|| \cdot . \sin(\alpha)\} \tag{2.4}$$

Given K and d, the ideal segmentation of data set X is the combination of $\{C_j\}$ and $\{F_j\}$ which minimizes the objective function below, where $C_j \subseteq X$, $C_j \cap C_i = \emptyset$, F_j is d dimensional linear space, and $1 \leq i, j \leq K$, $i \neq j$.

$$W_K = \sum_{j=1}^{K} \int_{u \in C_j} dist^2(u, F_j) du. \tag{2.5}$$

2.4.1 Two Lines

Assume we have two lines l_1 and l_2 within the unit disk in $\mathbb{R}^2$. They pass through the origin and the angle between them (the smaller one) is ϕ. Further we assume each line has *conic* noise with angle θ around it.

Then for $X = l_1 \cup l_2$, we obtain the following sequences $\{W_K\}$ from some algebraic

Algorithm 2 The Second Order Difference with equal but unknown dimension(SOD2)

Require: $X = \{\mathbf{x}_1, \mathbf{x}_2, \ldots, \mathbf{x}_N\} \subset \mathbb{R}^D$:data, d_{max}:the estimated largest dimension, K_{max}:the estimated largest number of clusters.

Ensure: $K_{d_{\text{SOD}}}$ disjoint cluster $C_1, \ldots, C_{K_{d_{\text{SOD}}}}$ which can be good approximated by d_{SOD} flats.

Steps:

for $d = 0, \ldots, d_{max} + 1$ **do**

Apply $SOD(d)$ (replace LBF by spectral clustering in SOD if $d = 0$) on X.
Record the output labels in $Labels\{d\}$.
Record the output K_{SOD} in K_d.
Record the output $W_{K_{\text{SOD}}}$ in W_d.

end for

Calculate $SOD(\ln W_d)$ by equation 2.2.
Find d_{SOD} by equation 2.3.
Return the labels $Labels\{d_{\text{SOD}}\}$ and $(d_{\text{SOD}}, K_{d_{\text{SOD}}})$.

computation:

$$\begin{aligned} W_1 &= \theta - \frac{\cos\phi \sin 2\theta}{2} \\ W_{2n} &= \theta - \frac{n \sin\frac{2\theta}{n}}{2} \\ W_{2n+1} &= \theta - \frac{n \sin\frac{2\theta}{n}}{4} - \frac{(n+1)\sin\frac{2\theta}{n+1}}{4} \end{aligned} \tag{2.6}$$

where $n = 1, 2, 3, \ldots$. And by basic algebra, we can show that if $\theta \ll \phi$, W_K has a big drop at $K = 2$. This is where the "elbow point" is and the $SOD(W)$ achieves the maximum. How $W_K, \ln W_K$ and their SOD behavior when $\theta = 0.1, \phi = \pi/3$ is shown in figure 2.1 (left).

2.4.2 Four Lines

Assume we have four lines l_1, l_2, l_3 and l_4 aligned in a clockwise order within a unit disk in $\mathbb{R}^2$. They all pass through the origin. While l_1 and l_2, and l_3 and l_4 have angle ϕ between them, l_2 and l_3 have angle $\frac{\pi}{2} - \phi$ between them. We also assume that each line has conic noise with angle θ around it and $0 < \theta \ll \phi < \frac{\pi}{4}$.

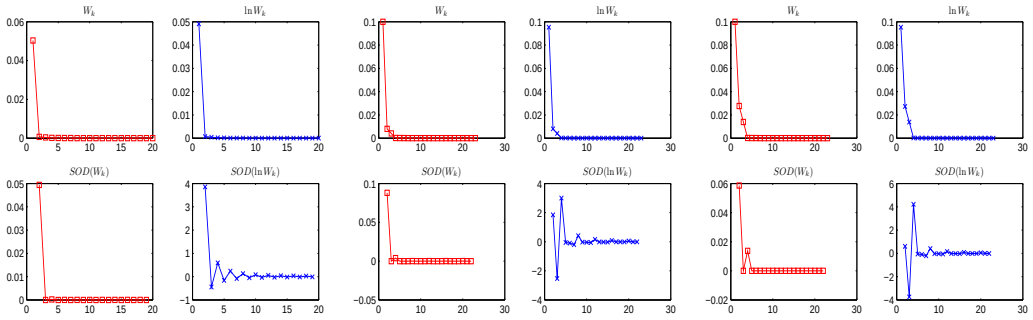

Figure 2.1: $W_K, \ln W_K$ *and their SOD from theoretical computation in different settings. 2 lines when* $\theta = 0.1, \phi = \pi/3$ *(left). 4 lines when* $\theta = 0.05, \phi = 23$ *degrees (middle) and 4 lines when* $\theta = 0.05, \phi = 42$ *degrees (right).*

Furthermore, assume we have ideal segmentation on $X = l_1 \cup l_2 \cup l_3 \cup l_4$. Then we get the sequences $\{W_K\}$ by algebra.

$$
\begin{aligned}
W_1 &= 2\theta \\
W_2 &= 2\theta - \cos\phi \sin 2\theta \\
W_3 &= 2\theta - \frac{\cos\phi \sin 2\theta}{2} - \frac{\sin 2\theta}{2} \\
W_{4n} &= 2\theta - n \sin \frac{2\theta}{n} \\
W_{4n+1} &= 2\theta - \frac{3n \sin \frac{2\theta}{n}}{4} - \frac{(n+1) \sin \frac{2\theta}{n+1}}{4} \\
W_{4n+2} &= 2\theta - \frac{n \sin \frac{2\theta}{n}}{2} - \frac{(n+1) \sin \frac{2\theta}{n+1}}{2} \\
W_{4n+3} &= 2\theta - \frac{n \sin \frac{2\theta}{n}}{4} - \frac{3(n+1) \sin \frac{2\theta}{n+1}}{4}
\end{aligned}
\tag{2.7}
$$

where $n = 1, 2, \ldots$. Apply SOD on W_K, we found that $SOD(W)_2 > SOD(W)_4$ for all $0 < \theta \ll \phi < \frac{\pi}{4}$. However, SOD of $\ln W_K$ can find 4 clusters at its maximum. We can see how the relevant values behavior when $\phi = 42$ and 23 degrees,$\theta = 0.05$ in figure 2.1 (middle and right).

Chapter 3

HLM Experiments

3.1 Numerical Experiments

3.1.1 Artificial Data

We compare SOD(given d), LED+SOD, SOD2, GPCA and ALC on a number of artificial data sets. In these experiments, data sets are generated by the Matlab code borrowed from the GPCA package on http://perception.csl.uiuc.edu/gpca. The data consisting of $100d$ samples lying in a unit cube are drawn from each subspace, corrupted with 0.05 gaussian noise. For the last four experiments, we restrict the angle between subspaces to be at least $\pi/8$ for separation. The LED+SOD first estimates dimension by LED and then applies SOD to estimate the number of clusters. We let $d_{max} = D - 1$ for SOD2, $K_{max} = 10$ for SOD (given d), LED+SOD and SOD2. We use spectral clustering as the segmentation method for $d = 0$ and LBF for other d. For GPCA, we embed the data to a $(d + 1)$ subspace by PCA and let the tolerance of rank detection be 0.05 [2, 1]. There is no automatic way to choose this tolerance, so we tried different values and picked the one which matched the ground truth the best.

Each experiment is repeated 100 times and the error rates of finding the dimension d, the number of clusters K, both and the computation time (in seconds) are recorded in Table 3.1.

As in table 3.1, SOD2 outperforms ALC(voting) in both accuracy and speed for artificial data. ALC with $\epsilon = 0.05$, which is the noise level can do a better job of finding

Table 3.1: The percentage of incorrectness ($e\%$) for finding the dimension d, the number of clusters K, both (d, K) and the computation time in seconds $t(s)$ of the methods SOD (given d), LED+SOD, SOD2, GPCA and ALC.

		no minimum angle							minimum angle $= \pi/8$			
	$e\%$	$1^6 \in \mathbb{R}^5$	$2^4 \in \mathbb{R}^5$	$3^3 \in \mathbb{R}^5$	$10^2 \in \mathbb{R}^{15}$	$1^6 \in \mathbb{R}^3$	$2^4 \in \mathbb{R}^3$	$3^3 \in \mathbb{R}^4$	$10^2 \in \mathbb{R}^{15}$	$1^6 \in \mathbb{R}^3$	$2^4 \in \mathbb{R}^3$	$3^3 \in \mathbb{R}^4$
SOD (LBF)	$e\%(K)$	17	3	2	0	55	29	19	0	3	5	5
(given d)	$t(s)$	3.51	4.07	3.37	7.31	3.13	3.77	3.85	6.78	3.09	3.45	3.32
	$e\%(d)$	2	0	3	10	10	4	7	7	4	1	5
SOD2	$e\%(K)$	17	4	6	11	59	42	16	7	4	12	8
(LBF)	$e\%(d, K)$	17	4	7	11	59	44	16	7	4	12	8
	$t(s)$	20.61	24.73	28.55	180.54	16.11	19.41	24.86	187.54	16.30	19.48	24.26
	$e\%(d)$	0	29	99	100	20	97	100	100	3	100	100
LED+SOD	$e\%(K)$	18	30	98	100	60	100	100	100	4	100	100
(LBF)	$e\%(d, K)$	18	30	99	100	60	100	100	100	4	100	100
	$t(s)$	6.82	8.53	8.97	53.06	5.60	8.95	10.75	53.95	5.72	8.14	10.83
ALC	$e\%(K)$	1	0	0	16	34	31	1	13	0	10	1
($\epsilon = 0.05$)	$t(s)$	23.74	43.44	59.14	1370.92	20.49	37.49	53.59	1354.11	20.22	37.41	54.11
ALC	$e\%(K)$	24	12	11	100	32	30	17	100	5	9	9
(voting)	$t(s)$	2094.75	2700.07	3530.26	119584.04	1207.54	2346.69	3628.24	117353.17	1184.08	2354.19	3956.05
GPCA	$e\%(K)$	88	100	100	100	27	100	100	100	13	100	100
	$t(s)$	0.03	0.09	0.12	1.30	0.06	0.09	0.12	1.30	0.04	0.09	0.12

the appropriate number of clusters. However, it still suffers in the running time when the subspaces are of high dimension and the noise level is usually unknown. SOD performs well and fast, but it requires the dimension as an input. LED+SOD and GPCA are fast, but they get unreasonable results for the artificial data.

3.1.2 Real Data

We also compare SOD, LED+SOD, SOD2, ALC and GPCA on some real data. We use 9 subsets of the Yale Face Database B consisting of face images of $2, \ldots, 10$ persons respectively under 64 varying lighting conditions. For computational efficiency, we follow [26] to downsample each image to 120×160 pixels, so the dimension of the image space is $D' = 120 \times 160$. We apply SVD to the data matrix to reduce the dimension to $D = 15$ for SOD and to $D = 10$ for the rest. The 9 subsets contain the faces with the following indices: [5, 8], [1, 5, 8], [1, 5, 8, 10], [1, 4, 5, 8, 10], [1, 2, 4, 5, 8, 10], [1, 2, 4, 5, 7, 8, 10], [1, 2, 4, 5, 7, 8, 9, 10], [1, 2, 3, 4, 5, 7, 8, 9, 10], [1, 2, 3, 4, 5, 6, 7, 8, 9, 10].

We let $K_{max} = 6, 8, 8, 10, 10, 12, 14, 16$ and 18 respectively for 2 to 10 clusters for SOD, LED+SOD and SOD2. For both LED+SOD and SOD2, we let $d_{max} = 6$. We get $d = 2$ by applying the dimension estimation method [32]. Thus we use $d = 2$ in SOD. Many other methods [32, 33, 34] will work as well since there is hardly any noise in face

data, but this was the easiest one for us to implement. For GPCA, we let tolerance be 0.05 which does not affect the performance in this experiment. For ALC (voting), we try different values from 10^{-5} to 10^{3} for ϵ and choose the estimated K by majority.

Each experiment is repeated 100 times and the error rate of finding the correct number of clusters, the mean and median of (d, K) and the computation time are recorded in Table 3.2.

Table 3.2: The percentage of incorrectness ($e\%$) for finding the correct number of clusters K, the mean $(\bar{d}, \bar{K})$, the median $(\tilde{d}, \tilde{K})$ of (d, K) and the computation time in seconds $t(s)$ of the methods SOD2 and LED.

Real K		2	3	4	5	6	7	8	9	10
SOD	$e\%(K)$	0	0	0	0	0	0	0	0	0
$(d = 2)$	$t(s)$	0.95	1.48	3.05	4.12	7.26	9.06	14.95	23.19	34.38
	$e\%(K)$	0	0	0	0	9	3	15	27	92
LED+SOD	$(\bar{d}, \bar{K})$	(3.00,2.00)	(3.00,3.00)	(3.00,4.00)	(3.00,5.00)	(3.00,6.15)	(3.00,6.94)	(3.00,7.54)	(3.00,7.93)	(3.00,7.28)
	$(\tilde{d}, \tilde{K})$	(3,2)	(3,3)	(3,4)	(3,5)	(3,6)	(3,7)	(3,8)	(3,9)	(3,7)
	$t(s)$	0.22	0.58	1.05	1.41	2.18	1.65	2.50	3.41	4.71
	$e\%(K)$	1	0	0	23	4	4	15	32	81
SOD2	$(\bar{d}, \bar{K})$	(4.96,2.03)	(4.18,3.00)	(4.43,4.00)	(3.33,5.27)	(4.10,6.07)	(3.94,6.92)	(3.48,7.71)	(3.55,8.44)	(3.70,8.23)
	$(\tilde{d}, \tilde{K})$	(5,2)	(5,3)	(5,4)	(4,5)	(4,6)	(4,7)	(3,8)	(3,9)	(4,8)
	$t(s)$	3.66	3.69	8.49	8.75	15.61	17.36	29.06	47.90	66.29
ALC	$e\%(K)$	0	0	0	0	0	0	0	0	0
(voting)	$t(s)$	80.02	196.16	355.07	563.61	828.80	1158.73	1530.74	1967.02	2490.59
GPCA	$e\%(K)$	100	0	100	100	100	100	100	100	100
	$t(s)$	0.07	0.13	0.52	0.71	1.02	1.56	2.70	2.65	3.38

LED+SOD had obvious advantage in speed and is accurate for small number of clusters (0% for $K \leq 5$). ALC has perfect detection but is slow. While SOD2 outputs reasonable values within moderate time.

Chapter 4

Robust Locally Linear Analysis

4.1 Robust PCA Algorithms

We discuss here algorithms for robust principal component analysis (robust PCA or RPCA) for recovering a given $m \times n$ matrix $\mathbf{X}$ when a percentage of the entries have been corrupted by noise. It is clear that in general, this is impossible: without some prior knowledge about the matrix, any value at any entry is as legitimate as any other value. However, it often happens in applications that $\mathbf{X}$ can be modeled as $\mathbf{X} = \mathbf{L} + \mathbf{S}$, where $\mathbf{L}$ is (approximately) low rank, and $\mathbf{S}$ is sparse. While RPCA in its broadest sense has a long history [35, 36], its intensive study with sparse corruption (as formulated above) only started recently with two parallel ground-breaking works by Candès et al. [17] and Chandrasekaran et al. [16]. They both proposed the following convex minimization for RPCA:

$$\min_{\mathbf{L} \in \mathbb{R}^{m \times n}} \|\mathbf{L}\|_* + \lambda \|\mathbf{X} - \mathbf{L}\|_1, \tag{4.1}$$

where $||\mathbf{X} - \mathbf{L}||_1 := \sum_{i,j} |\mathbf{X}_{ij} - \mathbf{L}_{ij}|$, $||\mathbf{L}||_*$ is the sum of the singular values of $\mathbf{L}$ (i.e., its nuclear norm) and λ is a fixed parameter. This minimization for RPCA is referred to by [17] as principal component pursuit (PCP)). Candès et al. [17] proved that if $\lambda = 1/\sqrt{n}$ and the data matrix can be represented as $\mathbf{X} = \mathbf{L}_0 + \mathbf{S}_0$, where $\mathbf{L}_0$ is low-rank and "strongly incoherent" (as specified in [17, eqs. (1.2)-(1.3)]) and $\mathbf{S}_0$ is sparse enough with uniformly sampled non-zero elements, then the minimizer of (4.1) is $\mathbf{L}_0$ with overwhelming probability (of the uniform sampling). On the other hand,

Chandrasekaran et al. [16] provided a condition for deterministic exact recovery for various distributions of corrupted elements, though it implied a stronger restriction on the fraction of corruption (see also [37] for weaker restrictions than [16]); clearly [16] could not fix λ for its more general setting.

Lin et al. [38] have implemented (4.1) via an augmented Lagrangian approach, which alternates between shrinkages of spaces and singular values. This procedure can be made very efficient when one has a good guess at an upper bound for the rank of the minimizer, which we refer as PCP(capped) and implement in the supplemental material (a similar idea of capping has appeared after the submission of this paper in [39]).

The PCP algorithm is only designed to deal with sparse errors and may not be stable to noise in all entries. For this purpose, Zhou et al. [40] proposed a stable PCP, which minimizes

$$\min_{\mathbf{L},\mathbf{S}\in\mathbb{R}^{m\times n}} \|\mathbf{L}\|_* + \lambda\|\mathbf{S}\|_1 + \frac{\nu}{2}\|\mathbf{X}-\mathbf{L}-\mathbf{S}\|_F^2. \tag{4.2}$$

A formally equivalent problem is

$$\min_{\mathbf{L},\mathbf{S}\in\mathbb{R}^{m\times n}} \|\mathbf{L}\|_* + \lambda\|\mathbf{S}\|_1 \text{ such that } \|\mathbf{X}-\mathbf{L}-\mathbf{S}\|_F \le \varepsilon. \tag{4.3}$$

They proved a perturbation-type result for the stability of the solution of (4.3) assuming the common condition for robustness of the solution of (4.1) and small values of noise ε (equivalently, large sizes of ν in (4.2); though there is no simple expression for the lower bound on ν in terms of the upper bound of ε). Other types of stability results appeared in [41] and [37]. However, in our setting of large noise (often larger than the signal when measured in Frobenius norm), such perturbation results may not be practical. Various methods are recently being proposed for solving this kind of optimization (see e.g., [42]), though we are not aware of any online code for this.

Another approach for RPCA, LMaFit [18], uses only the last two terms of (4.2). That is, it minimizes the objective function

$$\min_{\mathbf{B},\mathbf{C},\mathbf{S}} \|\mathbf{S}+\mathbf{BC}-\mathbf{X}\|_F^2 + \mu\|\mathbf{S}\|_1, \tag{4.4}$$

where $\mathbf{S}\in\mathbb{R}^{m\times n}$, $\mathbf{B}\in\mathbb{R}^{m\times d}$ and $\mathbf{C}\in\mathbb{R}^{d\times n}$. The LMaFit introduces narrow matrices $\mathbf{B}$ and $\mathbf{C}$ to control the rank of the approximation and allows distortion by adding the Frobenius norm term to the objective function. Similarly to stable PCP, the LMaFit model is expected to handle well Gaussian noise.

4.1.1 RPCA via an Alternating Least Squares Algorithm

The simplest interpretation of the decomposition of $\mathbf{X}$ into sparse $\mathbf{S}$ and low rank $\mathbf{L}$ is to fix the number of nonzero elements N_0 in $\mathbf{S}$ (or its percentage p, so that $N_0 = \lfloor p \cdot m \cdot n \rfloor$) and to fix a rank d for $\mathbf{L}$. In this situation, we might measure errors with some matrix norm. If we choose the Frobenius norm, following the notation above, we may get the problem

$$\min_{\mathbf{B},\mathbf{C},\mathbf{S}} \|\mathbf{S} + \mathbf{BC} - \mathbf{X}\|_F^2, \text{ s.t. } \|\mathbf{S}\|_0 \leq N_0. \tag{4.5}$$

Clearly, the LMAFit minimization of (4.4) is a relaxation of this problem.

We suggest a variant for the minimization of (4.5). We represent the set of corrupted indices by a matrix $\mathbf{W} \in \{0,1\}^{m \times n}$ with N_0 ones (for indices of corrupted points) and $m \cdot n - N_0$ zeros. We denote the Hadamard product by $\circ$, i.e., $(\mathbf{A} \circ \mathbf{B})_{ij} = \mathbf{A}_{ij}\mathbf{B}_{ij}$. Then, instead of minimizing (4.5), we may minimize the objective function $J(\mathbf{B}, \mathbf{C}, \mathbf{W}) = \|(\mathbf{BC} - \mathbf{X}) \circ \mathbf{W}\|_F^2$.

In order to obtain a well-conditioned optimization problem and thus stable solutions, we modify J by adding some regularization terms (depending on sufficiently small $\lambda_1 > 0$, $\lambda_2 > 0$, $\lambda_3 > 0$ and $\mathbf{U} \in \mathbb{R}^{m \times n}$ whose elements are i.i.d. samples from a continuous distribution on [0, 1]) as follows:

$$J(\mathbf{B}, \mathbf{C}, \mathbf{W}) = \|(\mathbf{BC} - \mathbf{X}) \circ \mathbf{W}\|_F^2 + \lambda_1 \|\mathbf{B}\|_F^2 + \lambda_2 \|\mathbf{C}\|_F^2 + \lambda_3 \|\mathbf{U} \circ \mathbf{W}\|_F^2. \tag{4.6}$$

The last term is useful more for theoretical than practical purposes, and we see no experimental benefit to adding it (see §6.1.2).

The low rank approximation is then $\mathbf{L} = \mathbf{B}\,\mathbf{C}$ and the sparse matrix $\mathbf{S} = \mathbf{X} - \mathbf{L}$ and is supported on the ones of $\mathbf{W}$. This formulation suggests a simple algorithm, which we describe in Algorithm 3 and will henceforth refer to as ALS. The idea is to iteratively minimize (4.6) alternating between minimization over $\mathbf{B}$ and $\mathbf{C}$ as well as estimating $\mathbf{W}$. The code has n_2 loops for re-evaluating $\mathbf{W}$ and n_1 loops for minimizing over $\mathbf{C}$ and $\mathbf{B}$.

Throughout all the experiments we fix the parameters of Algorithm 3 as follows: $\lambda_1 = \lambda_2 = \lambda_3 = 10^{-10}$ and form $\mathbf{U}$ by drawing i.i.d. samples from uniform distribution on [0, 1]. We also fix $n_1 = 1$. For the simulated data in § 6.1.1 n_2 is chosen such that either the algorithm converges or n_2 obtains a sufficiently large value. More precisely,

Algorithm 3 An ALS algorithm of recovering a low rank matrix from corrupted data

Input: $\mathbf{X} \in \mathbb{R}^{m\times n}$, d: low rank, p: the percentage of corrupted entries, n_1, n_2: numbers of iteration, $\lambda_1, \lambda_2, \lambda_3 \geq 0$: regularization parameters .
Output: $\mathbf{B} \in \mathbb{R}^{m\times d}$, $\mathbf{C} \in \mathbb{R}^{d\times n}$, $\mathbf{W} \in \{0,1\}^{m\times n}$ with exactly $\lfloor p \cdot m \cdot n \rfloor$ zeros.
Initialization: $\mathbf{W} = \mathbf{1}$, $\mathbf{B} \in \mathbb{R}^{m\times d}$ with i.i.d. entries: $\mathbf{B}_{ij} \sim \mathcal{N}(0,1)$, $\mathbf{U} \in \mathbb{R}^{m\times n}$ with i.i.d. entries: $\mathbf{U}_{ij} \sim \mathit{Uniform}(0,1)$.
for $l = 1 : n_2$ **do**
  for $t = 1 : n_1$ **do**
    $\mathbf{C} = \arg\min_{\mathbf{C}} J$ (J is defined in (4.6)).
    $\mathbf{B} = \arg\min_{\mathbf{B}} J$.
  end for
  $\mathbf{W}$ is 0 at the indices of the $\lfloor p \cdot m \cdot n \rfloor$ greatest elements of $\{|\mathbf{X}_{ij} - (\mathbf{BC})_{ij}|^2 + \lambda_3 \mathbf{U}_{ij}^2\}_{i=1\,j=1}^{m\quad n}$, and 1 otherwise.
end for

the outer loop stops if one of the following criterions is achieved: 1) $n_2 = 100$; 2) the relative change of J is less than 10^{-3}; 3) the absolute change of J is less than 10^{-4}. For the image data in §6.2 ALS is applied within K-ALS and it was enough to require $n_2 = 1$ and consequently speed up the algorithm. We note that the other parameters, p and d, have a clear interpretation in terms of the data and one may expect a bound on them for various data sets. More specifically, the results of ALS are robust to overestimation of p and d, but not robust to underestimation (see §6.1.2). In §6.1.3, we propose and test an estimation strategy for d. We demonstrate results on artificial data in §6.1.1, while in the main text we focus on the application of ALS within a hybrid linear modeling approach to both impulsive denoising and blind painting.

ALS algorithms for PCA have long history and have been widely used for matrix completion, i.e., when the locations of the corrupted elements are specified, see for example [43, 44, 45, 46, 47, 48, 49]. In fact, the ALS algorithm for matrix completion is practically obtained by fixing the matrix $\mathbf{W}$ according to known and missing locations (1's and 0's of this matrix) and performing a restricted version of the ALS algorithm of this paper.

4.1.2 Why a New RPCA Algorithm?

The reader may wonder why we use an alternating least squares method rather than the convex method of [16, 17] or its stable version [40], which have theoretical guarantees. We will use RPCA in a K-subspaces framework for modeling the underlying data by multiple subspaces. One cannot expect a fully convex formulation for such setting. Indeed, Lerman and Zhang [50, §5.1] have shown that it is impossible to generalize convex strategies as in [16, 17] for recovering multiple subspaces by energy minimization. Moreover, strategies like [51, 52], which generalize [16, 17] to obtain an affinity matrix via a convex procedure (and then apply the non-convex spectral clustering), are extremely slow for our application (see §6.2).

We were also unable to successfully apply [16, 17] (or its stable version) within a K-subspaces algorithm because it is not obvious how to extend the nuclear norm out-of-sample (see §4.2.2). In particular, we find it difficult to prove weak convergence theorems for the naive K-subspaces versions of PCP, unlike ALS (see §5.1.4), due to the lack of monotonicity. While [18] naturally generalizes to a K-subspace algorithm, our experimental results using their code in the setting of image denoising have not been succesful.

Finally, and in some sense, most importantly, in our image denoising application, we have a good initialization. One of the complaints with non-convex methods like ALS or K-subspaces is the dependence on the initialization for good performance. But the initialization of the dictionary as in [11] has shown to be effective for image denoising. In our setting, because we have such a good idea where to start, dependence on initialization is actually a feature, and not a bug.

4.2 Piecewise Linear Models

We introduce local versions of the ALS (and other low-rank modeling algorithms) for block structured dictionary learning. Alternatively, we introduce local linear modeling of data with low-dimensional structure in the presence of large and sparse corruption. Our elementwise matrix corruption model completely distorts the nearest neighbors' distances between the uncorrupted data points (stored as matrix columns). Therefore, standard methods for manifold learning [53, 54, 55] will completely fail on such corrupted

data. We thus model the data by several multiple subspaces via a K-subspaces strategy, which replaces the least squares best fit subspaces by different robust low-rank best fit subspaces.

4.2.1 The K-ALS Algorithm

The K-ALS algorithm aims to minimize the following regularized objective function:

$$\begin{aligned} J \quad & (\{\mathbf{B}_k\}_{k=1}^K, \{\mathbf{C}_k\}_{k=1}^K, \{\mathbf{W}_k\}_{k=1}^K, \eta) \qquad (4.7) \\ = \quad & \sum_{k=1}^{K} (\|(\mathbf{B}_k\mathbf{C}_k - \mathbf{X}_k) \circ \mathbf{W}_k\|_F^2 + \lambda_1\|\mathbf{B}_k\|_F^2 + \lambda_2\|\mathbf{C}_k\|_F^2 + \lambda_3\|\mathbf{U}_k \circ \mathbf{W}_k\|_F^2) + \lambda_4 \sum_{j=1}^{n} v_{\eta(j)}^2, \end{aligned}$$

where η maps the indices of data points $(1, \ldots, n)$ to indices of subspaces $(1, \ldots, K)$, $\mathbf{X}_k \in \mathbb{R}^{m \times n_k}$ is a submatrix of $\mathbf{X}$ representing the n_k data points in cluster $\eta(j) = k$, $\mathbf{W}_k \in \{0,1\}^{m \times n_k}$, $\mathbf{U}_k \in \mathbb{R}^{m \times n_k}$ and both $\{\mathbf{U}_k\}_{k=1}^K$ and $(v_1, \ldots, v_K)$ are initialized by i.i.d. samples from a continuous distribution on [0, 1]. The regularization parameters $\lambda_1, \ldots, \lambda_4$ are arbitrarily small and positive. Throughout all the experiments $\lambda_1 = \lambda_2 = \lambda_3 = \lambda_4 = 10^{-10}$. We have found that in practice one may consider $\lambda_3 = \lambda_4 = 0$, but all of these regularization constants are necessary for our theory.

In practice, K-ALS uses Lloyd's algorithm as follows. The input parameters of K-ALS are the number of subspaces, K, a rank, d (though mixed ranks for the different subspaces are also possible), a percentage of corrupted entries, p, regularization parameters $\lambda_1, \ldots, \lambda_4$, $\{\mathbf{U}_k\}_{k=1}^K$ and $(v_1, \ldots, v_K)$ and number of iterations n_1, n_2 and n_3. The algorithm first initializes a list of subspaces (details of the initialization for the imaging problems of this paper are discussed in §6.2). The algorithm first initializes the matrix $\mathbf{W}$ (with indices 1 for estimated corrupted coordinates and 0 for uncorrupted) The algorithm then iteratively repeats the following two steps n_3 times. The first step finds the nearest subspace to each data point, ignoring the entries currently suspected to be corrupted. That is, given a data point $\mathbf{x} \in \mathbb{R}^m$ (i.e., column of the matrix $\mathbf{X}$), let $\overline{\mathbf{x}}$ denote the suspected uncorrupted entries in $\mathbf{x}$. Furthermore, for each $1 \leq i \leq K$ and each such $\overline{\mathbf{x}}$ (obtained from a column of $\mathbf{X}$) let $\overline{\mathbf{B}}_i \equiv \overline{\mathbf{B}}_i(\overline{\mathbf{x}})$ be the $\dim(\overline{\mathbf{x}}) \times d$ matrix formed by the rows of $\mathbf{B}_i$ corresponding to the same uncorrupted indices of $\mathbf{x}$. Using this notation, $\mathbf{x}$ is nearest to the subspace indexed by

$$j = \underset{1 \leq i \leq K}{\arg\min} \min_{\mathbf{c} \in \mathbb{R}^d} \left(\|\overline{\mathbf{B}}_i \mathbf{c} - \overline{\mathbf{x}}\|_2^2 + \lambda_4 v_i^2 \right). \qquad (4.8)$$

The second step computes a new basis for each cluster of points assigned to a given subspace of the first step by the ALS procedure of §4.1 (we used the same notation for the parameters required by 3). Our implementation of the K-ALS algorithm is available on `http://www.math.umn.edu/~wangx857/kals`.

4.2.2 Other Possibilities of K-RPCA Algorithms

The generalization of the PCP model ($\|\cdot\|_* + \lambda \cdot \|\cdot\|_1$) to the setting of K-subspaces is less straightforward. Indeed, the inclusion of new data points (i.e., the first step above) affects the nuclear norm of the whole data set and may require changing the representations of other points. Nevertheless, to run the local version of the algorithm, if $\mathbf{x} \in \mathbb{R}^m$ is a data point and $\mathbf{B}_1, ..., \mathbf{B}_K$ are the orthonormal bases of the d-dimensional subspaces representing the clusters, then we associate to $\mathbf{x}$ the subspace $\mathbf{B}_j$, where

$$j = \arg\min_{1 \le i \le K} \min_{\mathbf{c} \in \mathbb{R}^d} \|\mathbf{x} - \mathbf{B}_i \mathbf{c}\|_1. \tag{4.9}$$

On the other hand, the LMaFit model extends to a K-LMaFit model without complications. If $\mathbf{x} \in \mathbb{R}^m$ is a data point and $\mathbf{B}_1, ..., \mathbf{B}_K$ are the orthonormal bases of the d-dimensional subspaces representing the clusters, then we associate to $\mathbf{x}$ the subspace $\mathbf{B}_j$, where

$$j = \arg\min_{1 \le i \le K} \min_{\mathbf{c} \in \mathbb{R}^d, \mathbf{e} \in \mathbb{R}^m} \left(\|\mathbf{e} + \mathbf{B}_i \mathbf{c} - \mathbf{x}\|_F^2 + \mu \|\mathbf{e}\|_1 \right). \tag{4.10}$$

4.2.3 Some Implementation Details

All the piecewise linear models discussed above have hard decision boundaries for cluster membership, therefore, points near the boundary may not be well represented. One simple remedy to this kind of problem is to repeat the clustering several times and generate multiple reconstructions via overlapping clusterings. In the wavelet literature, this technique is called cycle spinning [56]; in this context, it is simply the idea that the charts of a manifold (which may be part of a union of manifolds) should overlap. If the final goal is denoising, then we average the outputs of all repetitions.

In the K-PCP model, when computing the nearest low rank model for a data point, we need to cap the rank allowed for each of the models, else the model with the highest rank will become the representative for every point.

Chapter 5

Mathematical Analysis

5.1 Mathematical Analysis of Convergence

We establish theoretical analysis for the (regularized) ALS and K-ALS algorithms. Our numerical experiments indicated similar performance of these regularized versions and the original versions presented earlier.

5.1.1 Preliminaries

We associate to both the ALS algorithm and the K-ALS algorithm mappings from their input to their possible outputs. For the ALS algorithm each iteration at time t computes the values of a point $(\mathbf{B}^t, \mathbf{C}^t, \mathbf{W}^t)$. A domain for this point is $\mathcal{X} = \mathbb{R}^{m\times d} \times \mathbb{R}^{d\times n} \times \{0,1\}^{m\times n}$. For the K-ALS algorithm we denote for simplicity a point $(\{\mathbf{B}_k\}_{k=1}^K, \{\mathbf{C}_k\}_{k=1}^K, \{\mathbf{W}_k\}_{k=1}^K, \eta)$ by Ω. We also denote this point at iteration t by Ω^t. The domain $\mathcal{X}$ for points Ω is $\mathcal{X} = (\mathbb{R}^{m\times d})^K \times (\mathbb{R}^{d\times n})^K \times (\{0,1\}^{m\times n})^K \times \{1,\ldots,K\}^n$.

We describe each algorithm as a mapping ϕ from $\mathcal{X}$ to the partition set of $\mathcal{X}$, $\mathcal{P}(\mathcal{X})$ (including several possible results as we have no a priori knowledge of convergence). A *fixed point* of ϕ is a point $\mathbf{x} \in \mathcal{X}$ for which $\{\mathbf{x}\} = \phi(\mathbf{x})$. We express convergence properties of both ALS and K-ALS in terms of fixed points of their corresponding mapping ϕ. The convergence theorems are formulated in probability since these algorithms contain randomly initialized regularization components.

5.1.2 Theorem for the Convergence of ALS

We establish the following result for convergence of the regularized ALS algorithm for robust PCA.

Theorem 1. *The following statements hold with probability one of the ALS algorithm: 1) All accumulation points of the iterates* $\{(\mathbf{B}^t, \mathbf{C}^t, \mathbf{W}^t)\}_{t=1}^{\infty}$ *produced by this algorithm are its fixed points; 2)* $J(\mathbf{B}^t, \mathbf{C}^t, \mathbf{W}^t) \to J(\mathbf{B}^*, \mathbf{C}^*, \mathbf{W}^*)$ *as* $t \to \infty$*, where* $(\mathbf{B}^*, \mathbf{C}^*, \mathbf{W}^*)$ *is a fixed point; 3)* $\|(\mathbf{B}^{t+1}, \mathbf{C}^{t+1}, \mathbf{W}^{t+1}) - (\mathbf{B}^t, \mathbf{C}^t, \mathbf{W}^t)\| \to 0$ *as* $t \to \infty$*; and 4) either* $\{(\mathbf{B}^t, \mathbf{C}^t, \mathbf{W}^t)\}_{t=1}^{\infty}$ *converges or its accumulation points form a continuum.*

5.1.3 Main Theorem: Convergence of K-ALS

We establish the following result for convergence of the regularized K-ALS algorithm for robust PCA.

Theorem 2. *For the regularized* K*-ALS algorithm described above, the following statements hold with probability one: 1) All accumulation points of the iterates* $\{\Omega^t\}_{t=1}^{\infty}$ *produced by this algorithm are its fixed points; 2)* $J(\Omega^t) \to J(\Omega^*)$ *as* $t \to \infty$*, where* Ω^* *is a fixed point; 3)* $\|\Omega^t - \Omega^{t+1}\| \to 0$ *as* $t \to \infty$*; and 4) either* $\{\Omega^t\}_{t=1}^{\infty}$ *converges or the accumulation points form a continuum.*

5.1.4 Discussion on Statements of Theorems

The purpose of our theory is to guarantee convergence of the ALS and K-ALS algorithms. While the convergence is not fully guaranteed (when the accumulation points form a continuum), we note that also the theoretical guarantees for the agglomerative Lagrangian for PCP [38] are only formulated in terms of convergence of the objective function as we have in the second part of our theoretical statements (but they do not have results for convergence in norm).

The type of convergence we have for K-ALS is slightly weaker than the one of K-means or K-subspaces. For these algorithms one can prove convergence to a local minimum [57], whereas here we only prove convergence to a fixed point. The difference is that for K-means and K-subspaces, the best fit center or subspace is easily determined for each cluster, whereas the robust ALS only guarantees convergence for each cluster.

It is interesting to note that while K-PCP easily determines a subspace for each fixed cluster, we cannot guarantee convergence for the full algorithm (as in K-ALS). Indeed, K-PCP minimizes $||\mathbf{L}||_* + \lambda||\mathbf{X} - \mathbf{L}||_1$ within each cluster, but for the partition it minimizes $||\mathbf{X}-\mathbf{L}||_1$ among clusters (due to the difficulty of extending the nuclear norm out of sample). Therefore the resulting objective function for our formulation of K-PCP is not even guaranteed to be monotonic.

5.2 Further Analysis including Proofs

We analyze the performance of the ALS algorithm following the strategies of [58, 59].

5.2.1 Preliminaries

Notation

Let $\mathbf{1}_{m\times n}$ denote the $m \times n$ matrix whose elements are all equal to 1; $\mathbf{I}$ denote the identity matrix (whose dimension will be clear from the context) and $|\mathbf{A}|_0$ denote the number of nonzero elements of the matrix $\mathbf{A}$. We let $\mathbf{A}_{\cdot j}$ and $\mathbf{A}_{i\cdot}$ denote the j-th column and i-th row respectively of the matrix $\mathbf{A}$.

Point-to-Set Maps

Definition 1 (Point-to-Set Map)**.** *Given two sets $\mathcal{X}$,$\mathcal{Y}$, a point-to-set map Ω is a function Ω: $\mathcal{X} \to \mathcal{P}(\mathcal{Y})$. The composition of two point-to-set maps Ω_1: $\mathcal{X} \to \mathcal{P}(\mathcal{Y})$ and Ω_2: $\mathcal{Y} \to \mathcal{P}(\mathcal{Z})$ is defined by $(\Omega_2 \circ \Omega_1)(\mathbf{x}) = \bigcup_{\mathbf{y}\in\Omega_1(\mathbf{x})} \Omega_2(\mathbf{y})$.*

Definition 2 (Closed Map)**.** *A point-to-set map Ω is closed at $\hat{\mathbf{x}} \in \mathcal{X}$ if for any $\mathbf{y} \in \mathcal{P}(\mathcal{Y})$ created by a sequence $\{\mathbf{x}_k\} \subset \mathcal{X}$ such that $\mathbf{x}_k \to \hat{\mathbf{x}}$ and a sequence $\mathbf{y}_k \in \Omega(\mathbf{x}_k)$ such that $\mathbf{y}_k \to \hat{\mathbf{y}}$: $\hat{\mathbf{y}} \in \Omega(\hat{\mathbf{x}})$.*

Definition 3 (Fixed Point)**.** *A fixed point of the map $\Omega : \mathcal{X} \to \mathcal{P}(\mathcal{X})$ is a point $\mathbf{x}$ for which $\{\mathbf{x}\} = \Omega(\mathbf{x})$. A generalized fixed point of Ω is a point $\mathbf{x}$ for which $\mathbf{x} \in \Omega(\mathbf{x})$.*

Iterative Algorithms

An iterative algorithm is a point-to-set map $\Omega : \mathcal{X} \to \mathcal{P}(\mathcal{X})$. It generates a sequence of points via the rule $\mathbf{x}_{k+1} \in \Omega(\mathbf{x}_k)$, where $\mathbf{x}_0$ is a given initial point. Now, suppose that

$\phi : \mathcal{X} \to \mathbb{R}_+$ is a continuous, non-negative function. An algorithm Ω is *monotonic* with respect to ϕ whenever $\mathbf{y} \in \Omega(\mathbf{x})$ implies that $\phi(\mathbf{y}) \leq \phi(\mathbf{x})$. If, in addition, $\mathbf{y} \in \Omega(\mathbf{x})$ and $\phi(\mathbf{y}) = \phi(\mathbf{x})$ imply that $\mathbf{y} = \mathbf{x}$, then we say that the algorithm is *strictly monotonic*.

We review the following theorems on convergence of iterative algorithms.

Theorem 3 (Zangwill [60])**.** *Let Ω be an algorithm that is monotonic with respect to ϕ. Given an initial point $\mathbf{x}_0$, suppose that the algorithm generates a sequence $\{\mathbf{x}_k\}$ that lies in a compact set; then the sequence has at least one accumulation point $\hat{\mathbf{x}}$, and $\phi(\hat{\mathbf{x}}) = \lim \phi(\mathbf{x}_k)$. Moreover, if Ω is closed at $\hat{\mathbf{x}}$ then $\hat{\mathbf{x}}$ is a generalized fixed point of the algorithm.*

Theorem 4 (Meyer [61])**.** *Assume that the algorithm Ω is strictly monotonic with respect to ϕ and that it generates a sequence $\{\mathbf{x}_k\}$ which lies in a compact set. If Ω is closed at an accumulation point $\hat{\mathbf{x}}$, then $\hat{\mathbf{x}}$ is a fixed point of Ω. Moreover, if $\mathcal{X}$ is normed, then $\|\mathbf{x}_{k+1} - \mathbf{x}_k\| \to 0$. It follows that $\{\mathbf{x}_k\}$ converges in norm to $\hat{\mathbf{x}}$ or that the accumulation points of $\{\mathbf{x}_k\}$ form a continuum.*

Infimal Maps

For $\phi : \mathcal{X} \times \mathcal{Y} \to \mathbb{R}_+$, we define the *infimal map* $M_{\mathbf{y}} : \mathcal{X} \to \mathcal{P}(\mathcal{Y})$ by $M_{\mathbf{y}}(\mathbf{x}) = \arg\min_{\mathbf{y} \in \mathcal{Y}} \phi(\mathbf{x}, \mathbf{y})$. We similarly define $M_{\mathbf{x}} : \mathcal{Y} \to \mathcal{P}(\mathcal{X})$.

We will decompose our algorithms by infimal maps and use the following auxiliary lemmata in order to apply Theorems 3 and 4.

Theorem 5 (Dantzig-Folkman-Shapiro [62])**.** *If $\phi(\hat{\mathbf{x}}, \cdot)$ is continuous on $\mathcal{Y}$, then $M_{\mathbf{y}}$ is closed at $\hat{\mathbf{x}}$.*

Theorem 6 (Fiorot-Huard [63])**.** *If the infimal maps $M_{\mathbf{x}}$ and $M_{\mathbf{y}}$ are both single-valued then the algorithm $\Omega \triangleq M_{\mathbf{x}} \circ M_{\mathbf{y}}$ is strictly monotonic with respect to ϕ.*

5.2.2 The ALS Algorithm as a Point-to-Set Map

In ALS the energy function J of (4.6) serves as the function ϕ of §5.2.1. Clearly J is continuous on $\mathbb{R}^{m \times d} \times \mathbb{R}^{d \times n} \times \mathbb{R}^{m \times n}$. Let $\mathcal{F} := \{\mathbf{W} : \mathbf{W} \in \{0,1\}^{m \times n}, |\mathbf{W}|_0 = \lfloor (1-p)mn \rfloor\}$. We assume that $d < \min(m, n)$ and p is the estimated portion of corruptions. The ALS algorithm minimizes J among $(\mathbf{B}, \mathbf{C}, \mathbf{W}) \in \mathbb{R}^{m \times d} \times \mathbb{R}^{d \times n} \times \mathcal{F}$. Defining, $M_{\mathbf{B}}(\mathbf{C}, \mathbf{W}) =$

$\arg\min_{\mathbf{B}} J$, $M_{\mathbf{C}}(\mathbf{B}, \mathbf{W}) = \arg\min_{\mathbf{C}} J$ and $M_{\mathbf{W}}(\mathbf{B}, \mathbf{C}) = \arg\min_{\mathbf{W}\in\mathcal{F}} J$, we rewrite the ALS algorithm as

$$\Omega = M_{\mathbf{W}} \circ (M_{\mathbf{B}} \circ M_{\mathbf{C}})^t, \tag{5.1}$$

where t is the number of iterations of the inner loop.

5.2.3 Conclusion of Theorem 1

At each step, the ALS algorithm is composed of $2t + 1$ infimal maps as in (5.1). For fixed $\mathbf{B}$, the product map $\mathbf{C} \mapsto \mathbf{BC}$ is continuous and J is continuous w.r.t. $\mathbf{BC}$. Thus, $J(\mathbf{B}, \cdot, \mathbf{W})$ is continuous for fixed $\mathbf{B}$ and $\mathbf{W}$. As a result, Theorem 5 implies that both $M_{\mathbf{B}}$ and $M_{\mathbf{C}}$ are closed. Furthermore, $M_{\mathbf{W}}$ is closed because $\mathcal{F}$ is finite. Therefore, the ALS algorithm is closed. Lemmata 1 and 2, which are formulated and proved below, imply that the ALS algorithm can be decomposed by single-valued infimal maps. Therefore, in view of Theorem 6 the ALS algorithm is strictly monotonic. Consequently, $\lambda_1\|\mathbf{B}^t\|_F^2 + \lambda_2\|\mathbf{C}^t\|_F^2 \leq J(\mathbf{B}^t, \mathbf{C}^t, \mathbf{W}^t) < J(\mathbf{B}^0, \mathbf{C}^0, \mathbf{W}^0)$. Thus the iterates of ALS are uniformly bounded. Combining these observations with Theorem 4, we conclude Theorem 1.

Establishing Single Values for $M_{\mathbf{W}}$

Lemma 1. *If the elements of* $\mathbf{U}$ *are i.i.d. samples from a continuous distribution on* $[0, 1]$*, then the* $\lfloor p \cdot m \cdot n \rfloor$*-th and* $\lfloor p \cdot m \cdot n \rfloor + 1$*-th greatest elements of* $\{|(\mathbf{B}^t\mathbf{C}^t)_{ij} - \mathbf{X}_{ij}|^2 + \lambda_3\mathbf{U}_{ij}^2\}_{\substack{1\leq i\leq m \\ 1\leq j\leq n}}$ *are different with probability 1.*

Proof. Due to the independence and continuity of the distribution of $\mathbf{U}_{ij}$, we have

$$\begin{aligned} \mathbb{P} \quad \{ \quad & |(\mathbf{B}^t\mathbf{C}^t)_{ij} - \mathbf{X}_{ij}|^2 + \lambda_3\mathbf{U}_{ij}^2 = |(\mathbf{B}^t\mathbf{C}^t)_{i'j'} - \mathbf{X}_{i'j'}|^2 + \lambda_3\mathbf{U}_{i'j'}^2 \} \\ = \quad & \mathbb{P}\{\lambda_3(\mathbf{U}_{i'j'}^2 - \mathbf{U}_{ij}^2) = |(\mathbf{B}^t\mathbf{C}^t)_{ij} - \mathbf{X}_{ij}|^2 - |(\mathbf{B}^t\mathbf{C}^t)_{i'j'} - \mathbf{X}_{i'j'}|^2\} \\ = \quad & 0 \end{aligned} \tag{5.2}$$

□

Establishing Single Values for $M_{\mathbf{B}}$ and $M_{\mathbf{C}}$

Lemma 2. *The infimal maps* $M_{\mathbf{B}}$ *and* $M_{\mathbf{C}}$ *derived from* (4.6) *are single-valued.*

Proof. By the definition of infimal maps

$$\hat{\mathbf{B}} := M_{\mathbf{B}}(\mathbf{C}, \mathbf{W}) \quad = \quad \arg\min_{\mathbf{B}} \|(\mathbf{BC} - \mathbf{X}) \circ \mathbf{W}\|_F^2 + \lambda_1 \|\mathbf{B}\|_F^2 + \lambda_2 \|\mathbf{C}\|_F^2. \quad (5.3)$$

Let $\tilde{\mathbf{C}}_{(i)} = \mathbf{C} \circ (\mathbf{1}_{d\times 1}\mathbf{W}_{i\cdot})$ and $\tilde{\mathbf{X}} = \mathbf{X} \circ \mathbf{W}_{i\cdot}$. Then

$$\hat{\mathbf{B}}_{i\cdot} = \tilde{\mathbf{X}}_{i\cdot}\tilde{\mathbf{C}}_{(i)}^T(\tilde{\mathbf{C}}_{(i)}\tilde{\mathbf{C}}_{(i)}^T + \lambda_1 \mathbf{I})^{-1}, \quad (5.4)$$

where $i = 1, \ldots, m$. Similarly, let $\hat{\mathbf{C}} = M_{\mathbf{C}}$ and we have

$$\hat{\mathbf{C}}_{\cdot j} = (\tilde{\mathbf{B}}_{(j)}^T\tilde{\mathbf{B}}_{(j)} + \lambda_2 \mathbf{I})^{-1}\tilde{\mathbf{B}}_{(j)}^T\tilde{\mathbf{X}}_{\cdot j}, \quad (5.5)$$

where $\tilde{\mathbf{B}}_{(j)} = \mathbf{B} \circ (\mathbf{W}_{\cdot j}\mathbf{1}_{1\times d})$ and $j = 1, \ldots, n$. Then (5.4) and (5.5) complete the proof. □

5.2.4 Conclusion of Theorem 2

The K-ALS algorithm can also be viewed as a point-to-set map:

$$\Omega = (M_{\mathbf{W}} \circ (M_{\mathbf{B}} \circ M_{\mathbf{C}})^{t_1})^{t_2} \circ M_\eta, \quad (5.6)$$

where $M_\eta = \arg\min_\eta J$, i.e.,

$$\eta(j) = \arg\min_k \min_{\mathbf{c}} \|(\mathbf{B}_k\mathbf{c} - \mathbf{X}_{\cdot j}) \circ \mathbf{W}_{\cdot j}\|_2^2 + \lambda_4 \mathbf{V}_{kj}^2, \quad (5.7)$$

where $\mathbf{W} = \mathbf{P}[\mathbf{W}_1 \ldots \mathbf{W}_K]$ and $\mathbf{P}$ is a permutation matrix such that $\mathbf{X} = \mathbf{P}[\mathbf{X}_1 \ldots \mathbf{X}_K]$.

The proof of Theorem 2 is analogous to Theorem 1. It suffices to show that (5.7) is single-valued. Because each element of $\mathbf{V}$ is i.i.d. sampled from a continuous distribution on [0, 1], we have:

$$\begin{aligned} \mathbb{P} \quad \{ \quad & \min_{\mathbf{c}} \|(\mathbf{B}_k\mathbf{c} - \mathbf{X}_{\cdot j}) \circ \mathbf{W}_{\cdot j}\|_2^2 + \lambda_4 \mathbf{V}_{kj}^2 = \min_{\mathbf{c}} \|(\mathbf{B}_{k'}\mathbf{c} - \mathbf{X}_{\cdot j}) \circ \mathbf{W}_{\cdot j}\|_2^2 + \lambda_4 \mathbf{V}_{k'j}^2 \, \} \\ = \quad & \mathbb{P}\{\lambda_4(\mathbf{V}_{k'j}^2 - \mathbf{V}_{kj}^2) = \|(\mathbf{B}_k\mathbf{c} - \mathbf{X}_{\cdot j}) \circ \mathbf{W}_{\cdot j}\|_2^2 - \|(\mathbf{B}_{k'}\mathbf{c} - \mathbf{X}_{\cdot j}) \circ \mathbf{W}_{\cdot j}\|_2^2\} \\ = \quad & 0 \end{aligned} \quad (5.8)$$

Therefore, (5.7) is single-valued with probability 1 and the theorem is concluded.

Chapter 6

Experiments

6.1 Numerical Experiments for ALS Algorithm

6.1.1 Numerical Simulations with a Single Subspace

To evaluate the performance of ALS in comparison to other RPCA methods, several simulations are conducted. We distinguish here and thereafter between p_0, the ground truth percentage of sparse corruptions (i.e., percentage of impulsive noise), and p, the input parameter of ALS estimating the percentage of corruption; d_0, the ground truth rank of the clean matrix, and d, the input rank of the matrices $\mathbf{B}$ and $\mathbf{C}$ for the ALS algorithm.

We generate a low rank matrix $\mathbf{X}_0$ as a product of two independent $mx \times d_0$ and $d_0 \times n$ matrices whose entries are i.i.d. $\mathcal{N}(0,1)$ random variables and scale it to have unit spectral norm. Due to the randomness, we repeat the experiment 100 times. We form $\mathbf{X}$ by independently adding to each element of $\mathbf{X}_0$ Gaussian noise with standard deviation σ (where $\sigma = 0.05$ or $\sigma = 0$ when no Gaussian noise). Finally, p_0 randomly chosen pixels of $\mathbf{X}$ ($p_0 = 5\%, 10\%, 20\%$) are assigned uniform random values in the interval $[-a, a]$, where $a = \max_{i,j} |\mathbf{X}_{0ij}|$.

We test the following RPCA algorithms on this data: PCP, PCP(capped), stablePCP, stablePCP(capped), LMaFit and ALS. All of our implementations appear in the supplementary material. For PCP, we use the fast implementation suggested in [38] with $\lambda = (mn)^{-0.25}$. We recall that PCP(capped) is the version of PCP mentioned in

§4.1, which requires an upper bound, i.e., a cap, on the intrinsic dimension. Since we are not aware of any available code for minimizing (4.2), we have implemented it by simple alternation (solving for each variable separately) and refer to this implementation as stablePCP. Its capped version is similar to that of PCP (but does not require the parameter γ).

For ALS, PCP(capped), stablePCP(capped) and LMaFit(oracle) we input the intrinsic rank to be $d_0 + 3$ (since they all can handle an overestimation for this parameter; see §6.1.2). For PCP(capped) we input in addition to λ of (4.1) a parameter γ, which is present in every ADMM (alternating direction method of multipliers) implementation for PCP (see supplemental code). We tested $(\lambda, \gamma) = (10^k, 10^l)$, for $k, l = -3, \ldots, 3$ and selected $(\lambda, \gamma) = (0.1, 10)$ based on the true fitting error (defined below); therefore our implementation of PCP(capped) is of oracle type. For stable(PCP) and stablePCP(capped), we tested $(\lambda, \nu) = (10^k, 10^l)$ for $k, l = -3, \ldots, 3$ and selected $(\lambda, \nu) = (0.1, 100)$ (thus stable(PCP) and stablePCP(capped) are also of oracle type). For LMaFit, we chose $\mu = 10^3$ by minimizing the true fitting error among $\mu = 10^k$, $k = -3, \ldots, 5$. We thus refer to the method as LMaFit(oracle). The parameters for ALS were specified in §4.1.1.

For all of the experiments $n = 1000$. For any RPCA algorithm, we quantify the recovery of the underlying low rank model by the following relative fitting error:

$$e = \frac{\|\tilde{\mathbf{X}} - \mathbf{X}_0\|_F}{\|\mathbf{X}_0\|_F}, \tag{6.1}$$

where $\tilde{\mathbf{X}}$ is the low rank estimation for X. We report the mean of this error (for the 100 different times the data was randomly generated) and for fixed values of m , d_0 and p_0 in Tables 6.1 and 6.2 when $\sigma = 0$ and $\sigma = 0.05$ respectively. Note that in those tables, the error is shown in percentage (%), ALS(p_0) inputs p_0 as the estimate of portion of corruptions, i.e., $p = p_0$, while ALS($2p_0$) has $p = 2p_0$.

We observe that PCP performs the best for clean data, but it could not handle well Gaussian noise. ALS works better with higher ambient dimensions, since in this case there are more equations for the least squares solution (with the same number of variables) and thus it increases the accuracy. ALS is also more accurate when the portion of corruptions decreases. We note that ALS(p_0) performs better than LMaFit(oracle) for clean data and they are comparable for noisy data. As for ALS($2p_0$), it performs better

Table 6.1: Mean relative fitting error (in percentage) on simulations without Gaussian noise. The random data matrix (generated 100 times) is $m \times 1000$ and its underlying rank is d_0. It is corrupted by p_0 sparse noise (random values).

m	100			200			400			800		
d_0	5			10			20			40		
p_0	5%	10%	20%	5%	10%	20%	5%	10%	20%	5%	10%	20%
ALS($2p_0$)	1.10	6.02	20.95	0.49	2.58	10.71	0.08	0.49	5.48	0.04	0.06	1.19
ALS(p_0)	0.15	0.54	2.93	0.02	0.05	0.66	**0.00**	**0.01**	0.11	**0.00**	**0.01**	0.02
PCP(capped)	0.43	6.56	19.86	0.44	3.69	10.97	0.61	2.51	5.93	0.90	2.60	5.35
PCP	**0.01**	**0.01**	**0.01**	**0.01**	**0.01**	**0.01**	0.01	**0.01**	**0.01**	0.01	**0.01**	**0.01**
LMaFit(oracle)	0.95	1.43	3.77	1.01	1.54	2.47	1.13	1.71	2.80	1.36	2.05	3.34
stable PCP	1.48	1.96	5.84	1.58	1.99	13.83	1.81	3.52	79.37	2.70	53.66	132.42
stablePCP(capped)	1.44	1.87	4.88	1.59	2.00	3.41	1.80	2.51	5.16	2.18	3.30	6.43

Table 6.2: Mean relative fitting error (in percentage) on simulations with Gaussian noise ($\sigma = 0.05$). The data matrix is $m \times 1000$ and its underlying rank is d_0. It is corrupted by additive Gaussian noise and p_0 sparse noise (random values).

m	100			200			400			800		
d_0	5			10			20			40		
p_0	5%	10%	20%	5%	10%	20%	5%	10%	20%	5%	10%	20%
ALS($2p_0$)	7.53	9.21	21.60	6.60	7.82	12.70	6.06	7.13	10.32	5.87	6.91	10.00
ALS(p_0)	6.65	7.04	8.63	5.80	6.13	6.84	5.28	**5.56**	**6.19**	**5.09**	**5.36**	**5.97**
PCP(capped)	14.27	15.31	20.56	11.89	12.74	14.91	10.03	10.74	12.43	8.74	9.41	10.95
PCP	20.80	24.37	41.59	15.86	18.97	26.25	12.40	13.34	17.61	10.28	11.50	14.43
LMaFit(oracle)	**5.38**	**5.84**	**6.95**	**5.23**	**5.69**	**6.79**	**5.11**	**5.56**	6.69	5.14	5.65	6.90
stable PCP	8.32	9.76	17.24	10.60	13.26	31.06	13.64	22.85	84.08	20.29	61.08	133.21
stablePCP(capped)	7.52	8.52	14.17	6.65	7.53	10.49	6.10	7.03	9.98	5.81	6.74	10.01

than PCP(capped) in general. When the ambient dimension is high or the corruption level is low then it performs better than LMaFit(oracle) for clean data and comparably to it for noisy data, whereas for the rest of the cases it is not as good as LMaFit(oracle).

Table 6.3 reports the speed of these algorithms with $\sigma = 0.05$ (the running times are comparable when $\sigma = 0$). The experiments were performed using a Dual processor Intel Core 2 CPU at 2.66GHz with 2 GB of memory. We observe that PCP(capped) is the fastest method (though we did not take into account the repetitions for the choices of the oracle parameters) and ALS is right after it. LMaFit is also comparable to these two in terms of speed (again repetitions for best parameters were not taken into account). On the other hand, PCP is extremely slow.

Table 6.3: The mean running times (in seconds) of the simulations with Gaussian noise ($\sigma = 0.05$). The data matrix is $m \times 1000$ and its underlying rank is d_0. It is corrupted by additive Gaussian noise and p_0 sparse noise (random values).

m	100			200			400			800		
d_0	5			10			20			40		
p_0	5%	10%	20%	5%	10%	20%	5%	10%	20%	5%	10%	20%
ALS($2p_0$)	0.18	0.17	0.18	0.48	0.50	0.48	0.84	0.81	0.80	2.14	2.10	2.04
ALS(p_0)	0.18	0.18	0.18	0.49	0.49	0.50	0.84	0.83	0.82	2.16	2.15	2.10
PCP(capped)	0.06	0.06	0.06	0.18	0.18	0.19	0.34	0.32	0.33	0.78	0.78	0.78
PCP	4.83	4.81	5.21	16.54	16.42	16.15	89.94	86.61	83.94	581.77	569.24	555.28
LMaFit(oracle)	0.26	0.31	0.46	0.56	0.66	0.93	0.93	1.10	1.54	1.79	2.17	3.11
stable PCP	1.32	1.36	1.50	4.05	4.42	5.24	26.04	30.20	91.69	172.03	539.39	775.11
stablePCP(capped)	0.71	0.74	0.83	2.10	2.24	2.68	11.18	11.93	14.74	61.04	64.75	81.20

6.1.2 Effect of the Parameters of ALS

We experimentally demonstrate the dependence of the ALS algorithm on the modeling parameters p and d and the regularization parameters λ_1, λ_2 and λ_3. Figures 6.3 and 6.4 plot the relative fitting error versus p for different experimental settings with fixed $d = d_0 + 3$ ($\lambda_1 = \lambda_2 = \lambda_3 = 10^{-10}$ here and below, unless specified). Each subfigure has a different value of m, d_0 and p_0, where $\sigma = 0$ in Figure 6.3 and $\sigma = 0.05$ in Figure 6.4. Figures 6.5 and 6.6 plot the relative fitting error versus d for ALS($2p_0$), ALS(p_0), PCP(capped) and LMaFit(oracle) with similar difference of the subfigures. We conclude from these figures that the ALS algorithm tends to be robust to the overestimation of the rank and it also allows the overestimation of p to some degree. The ALS algorithm is less robust to the underestimation of these two parameters, however, it can still perform

well under very mild underestimation.

In order to test the effect of the regularization parameters in ALS, we set $\lambda_1 = \lambda_2 = \lambda_3 = 10^k$, where $k = -4, \ldots, -16$. We found that ALS is stable w.r.t. both accuracy and speed when λ_1, λ_2 and λ_3 are sufficiently small. The accuracy and speed for one scenarios are displayed in Figure 6.1 and 6.2 respectively.

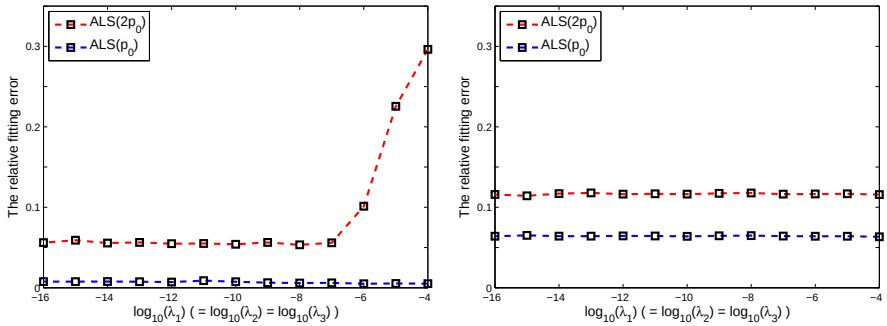

Figure 6.1: The relative fitting error for the ALS algorithm with different values of the regularization parameters λ_1, λ_2 and λ_3. The left figure is without Gaussian noise and the right one is with Gaussian noise ($\sigma = 0.05$). The ALS algorithm seems to be robust to the choice of the regularization parameters if they are sufficiently small.

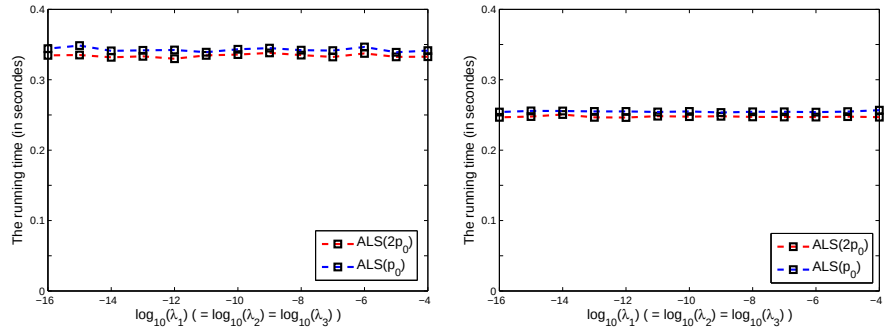

Figure 6.2: The running time for the ALS algorithm with different values of the regularization parameters λ_1, λ_2 and λ_3. The left figure is without Gaussian noise and the right one is with Gaussian noise ($\sigma = 0.05$). The choice of regularization parameters does not affect the speed of the algorithm.

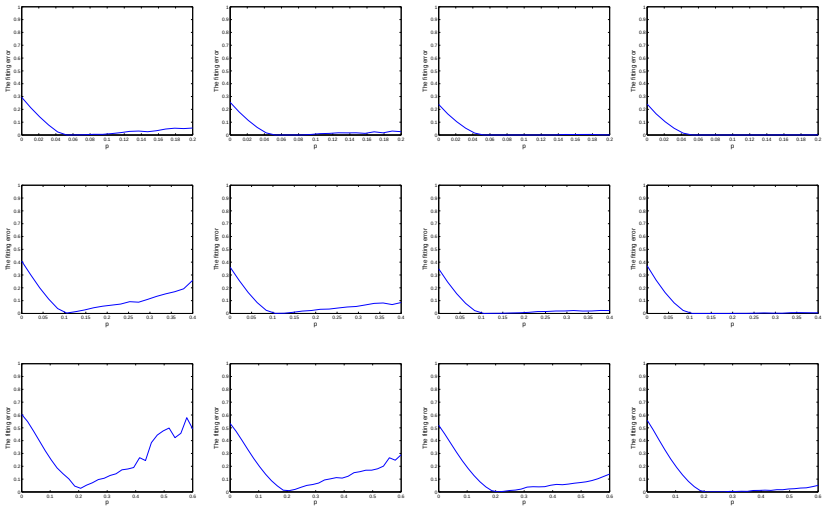

Figure 6.3: The performance of the ALS algorithm for different values of the parameter p without Gaussian noise. In each figure, the mean relative fitting errors are plotted versus p for different settings, where the data matrix is $m \times 1000$, its underlying rank is $m/20$ and the data matrix is corrupted by p_0 sparse (or impulsive) noise. From top to bottom, $p_0 = 0.05, 0.1$ and 0.2 respectively. From left to right, $m = 100, 200, 400$ and 800 respectively. The ALS algorithm seems to be robust to overestimation of p, especially when the ambient dimension (m) is large.

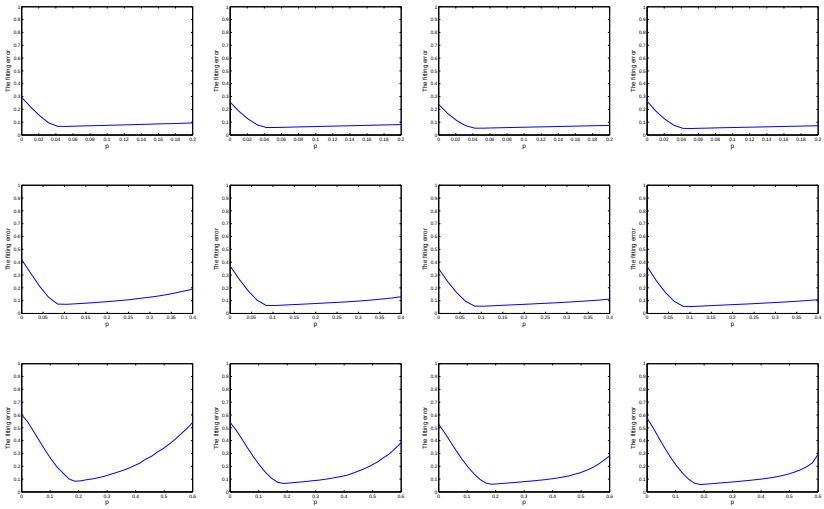

Figure 6.4: The performance of the ALS algorithm for different values of the parameter p with Gaussian noise ($\sigma = 0.05$). In each figure, the mean relative fitting errors are plotted versus p for different settings, where the data matrix is $m \times 1000$, its underlying rank is $m/20$ and the data matrix is corrupted by p_0 sparse (or impulsive) noise and additive Gaussian noise. From top to bottom, $p_0 = 0.05, 0.1$ and 0.2 respectively. From left to right, $m = 100, 200, 400$ and 800 respectively. The ALS algorithm seems to be robust to overestimation of p, especially when the ambient dimension (m) is large.

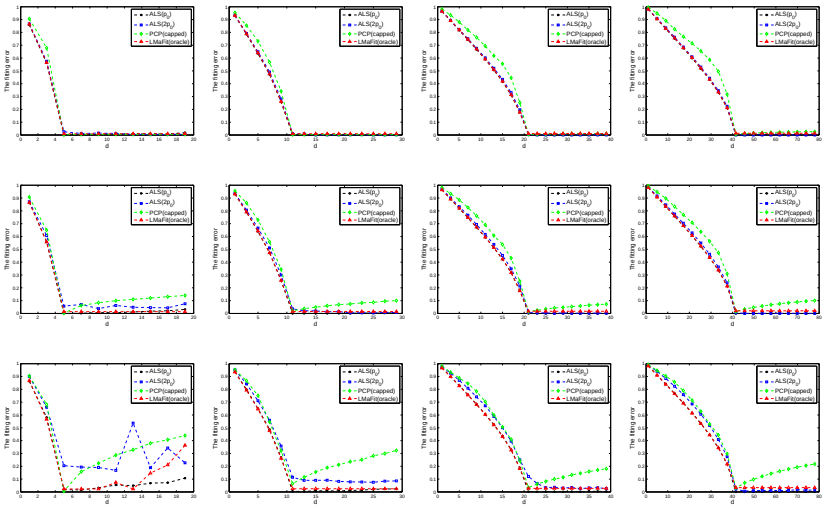

Figure 6.5: The effect of the parameter d on the performance of algorithms ALS($2p_0$), ALS(p_0), PCP(capped) and LMaFit(oracle) without Gaussian noise. In each figure, the relative fitting errors are plotted versus d for different settings, where the data matrix is $m \times 1000$, its underlying rank is $d_0 = m/20$ and the data matrix is corrupted by p_0 sparse (or impulsive) noise. From top to bottom, $p_0 = 0.05, 0.1$ and 0.2 respectively. From left to right, $m = 100, 200, 400$ and 800 respectively. The ALS algorithm is robust to overestimation of d, especially when the ambient dimension (m) is large.

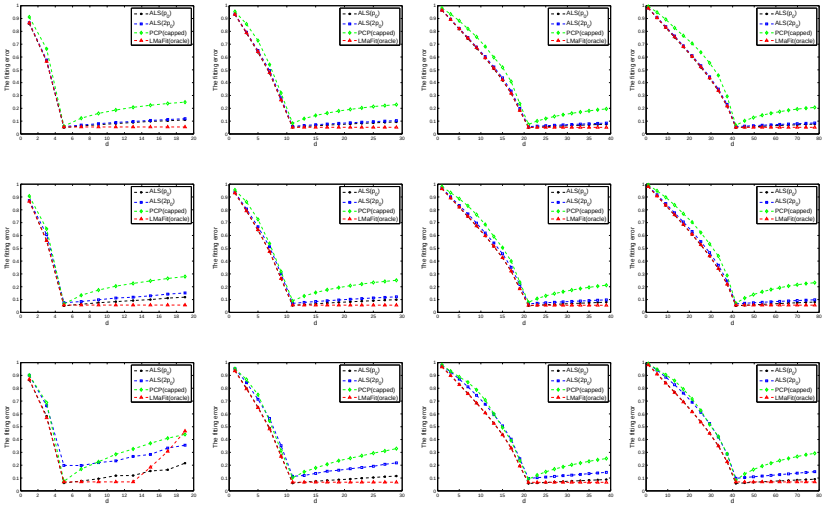

Figure 6.6: The effect of the parameter d on the performance of algorithms ALS($2p_0$), ALS(p_0), PCP(capped) and LMaFit(oracle) with Gaussian noise ($\sigma = 0.05$). In each figure, the relative fitting errors are plotted versus d for different settings, where the data matrix is $m \times 1000$, its underlying rank is $d_0 = m/20$ and the data matrix is corrupted by p_0 sparse (or impulsive) noise and additive Gaussian noise. From top to bottom, $p_0 = 0.05, 0.1$ and 0.2 respectively. From left to right, $m = 100, 200, 400$ and 800 respectively. The ALS algorithm is robust to overestimation of d, especially when the ambient dimension (m) is large.

6.1.3 Estimation of the Rank in ALS

Since ALS is robust to overestimation of the rank, we suggest the following strategy to estimate the underlying low rank of a corrupted matrix. We apply ALS with an increasing sequence of dimensions $d_1 < \ldots < d_t$ and denote the corresponding low-rank estimators of $\mathbf{X}$ by $\tilde{\mathbf{X}}_1, \ldots, \tilde{\mathbf{X}}_t$. We then estimate the ranks of these estimators and denote them by $\tilde{d}_1, \ldots, \tilde{d}_t$ respectively. This estimated sequence would increase first, be equal to the underlying rank d_0 for a while and finally increase again because of the corruptions. Finding the "stable phase" (i.e., when the sequence does not increase) will determine the appropriate rank.

To estimate the ranks of the different estimators, we apply second order differences (SODs) to detect abrupt changes in the singular values of these estimators. Indeed, if the underlying rank of a matrix is r, then the top $(r+1)$ singular values of the matrix drop very quickly, while the ones following them decrease more slowly. The SOD of the singular values thus expect to indicate the maximum at $r+1$. If $\sigma_1, \ldots, \sigma_m$ are the singular values of an $m \times n$ estimator (assume $m < n$ WLOG), then the SODs obtain the form:

$$S(i) = \sigma_{i-1} + \sigma_{i+1} - 2\sigma_i, \; i = 2, \ldots, m-1, \tag{6.2}$$

and the estimated rank $\hat{d}$ can be expressed by

$$\hat{d} = \arg\max_i S(i) - 1. \tag{6.3}$$

Note that this procedure is not able to detect the rank of a matrix if $r \geq m-2$. However, in most problems where the rank is relatively low, this is not the case.

We estimated the rank for the synthetic setting of §6.1.1. We chose an arithmetic sequence $\{d_i\}_{i=1}^{20}$ such that $d_1 = 1$ and $d_{20} = 0.2 \cdot m$. We compared with the rank estimated by PCP and PCP(capped), where the cap for PCP(capped) was $0.2 \cdot m$. We considered both output values of d_0 and d_0+1 as successes (after all, ALS is not sensitive to overestimation and the estimated ranks were either no greater than $d_0 + 1$ or equal to d_{20}). All synthetic scenarios were repeated 100 times. We found out that these three methods worked well: PCP worked perfectly; ALS only made one mistake (out of 100) when $m = 100$, $p = 20\%$ and Gaussian noise was added; PCP(capped) was correct around 75% of the random samples, when $m = 100$, $p = 20\%$ and no Gaussian noise

added and when $m = 100, 200$ and $p = 20\%$ with Gaussian noise and was 100% correct otherwise.

6.2 Restoration of Corrupted Images

6.2.1 Problem Setting

We test different methods of local (and global) low rank modeling for denoising images with impulsive noise as well as blind inpainting. The data consists of 5 popular images and also the 100 test images of the Berkeley Segmentation Database (BSD) [64]. The images are corrupted with i.i.d. additive Gaussian noise with standard deviation σ, and a percentage of p_0 random pixels per image (uniformly selected) are corrupted with integers uniformly sampled between 0 and 255. For inpainting, the images are further degraded by drawing a scratch. For many of the methods (in particular, K-ALS) the images are represented by their 8×8 patches. That is, the actual data matrix $\mathbf{X}$ is formed by stacking the vectors representing these patches as columns. Its size is thus $64 \times n$, where n is the number of pixels in the image. This matrix is transformed back to the image (after enhancing it) by finding the average value of all coordinates representing the same pixel.

6.2.2 Methods, Implementation Details and Parameters

We compared K-ALS with the following methods (sometimes combined with each other, though we reported only methods that were sufficiently fast and accurate): Median filter (MF), iterated median filter (IMF), structured sparse model selection (SSMS) [11], K-SVD [10, 65], low rank representation (LRR) [51, 52], PCP, PCP (capped), LMaFit, K-PCP, K-PCP(capped), K-LMaFit and two variations (NL-Median1 and NL-Median2) of the non-local means method of [66]. When two methods are combined, we use "+" to connect them, e.g. MF+SSMS, which means we apply SSMS after MF.

We explain here various implementation issues of the different algorithms and the choice of parameters. For IMF, we chose among 10 iterations the one with highest PSNR, thus giving an oracle advantage to this method. For local methods based on the K-subspaces strategy (i.e., SSMS, K-ALS, K-PCP, K-LMaFit), we followed [11] to learn

$K = 19$ subspaces of dimension $d = 8$ with 18 bases for subspaces initialized on artificial edges at given orientations and one low frequency DCT basis (our implementation is available online). Note that this initialization is important for good results.

In order to account for Gaussian noise, we apply additional steps in the spirit of [11] (in order to be consistent for all methods). We first recall that [11] uses the following thresholding step for their estimator for $\mathbf{X}$, $\tilde{\mathbf{X}}$, in order to remove additional Gaussian noise. The modified estimator $\hat{\mathbf{X}}$ is obtained by replacing each column $\tilde{\mathbf{x}}$ of $\tilde{\mathbf{X}}$ by the following column:

$$\hat{\mathbf{x}} = \mathbf{B}\delta(\mathbf{B}^T\tilde{\mathbf{x}}), \tag{6.4}$$

where $\mathbf{B} \in \mathbb{R}^{m\times d'}$ is formed by stacking as columns the first d' components of the basis of the cluster containing $\tilde{\mathbf{x}}$ (they use the full dimension $d' = 64$) and for $\mathbf{a} = (a_1, \ldots, a_{d'})$ and $1 \leq j \leq d'$: $(\delta(\mathbf{a}))_j = a_j$ if $|a_j| > 3\sigma$; and $= 0$ otherwise (i.e., SSMS assumes knowledge of the model parameter σ described in §6.2.1).

For K-ALS and K-PCP we applied a similar thresholding procedure within each iteration with $d' = 20$. We chose this parameter since the SVD of the clusters of natural image patches can be well approximated with rank 15 and slight overestimation cannot effect the results.

Before thresholding, K-ALS applies the following procedure within each iteration to re-estimate the locations of corruption in the corresponding image: let $\mathbf{Y}$ denote the original image, $\text{med}(\mathbf{Y})$ the image obtained by applying the 4×4 median filter to $\mathbf{Y}$, $\tilde{\mathbf{Y}}$ the image translated from the patches of the current iteration (before thresholding) and $\text{abs}(\cdot)$ the elementwise absolute value. Furthermore, let $r = \text{abs}(\mathbf{Y} - \tilde{\mathbf{Y}})$ and $s = \text{abs}(\mathbf{Y} - \text{med}(\mathbf{Y}))$. For denoising, we identify in each iteration the corrupted pixels of a fixed percentage (p) as the ones with the largest entries in r; for inpainting, we do the same with $r + s$ at the first iteration and with r thereafter (the purpose of the additional s for inpainting is to improve scratch detection, however, for denoising such a process can falsely detect edges as corruption). This update of $\mathbf{W}$ is very natural in the framework of K-ALS; K-ALS has the advantage of using application-dependent information in the estimate of locations of corrupted elements.

For the global low rank model (in particular, PCP), we address Gaussian noise by further applying the SSMS algorithm [11] (so the method is comparable to the other strategies). Numerical experiments indicated that applying SSMS after the global low

rank model was slightly better than applying the thresholding described above and clearly better than PCP alone. We did not notice an advantage of stablePCP over PCP and did not report it since it required experimentation with the additional parameter ν.

We describe in §6.2.3 two robust variants of the non-local means algorithm [66]. We have also tested the median variant of the non-local means toolbox on Matlab exchange [67], however, its performance was not satisfying and is thus not reported here.

For LRR [51, 52], it is not feasible to assign the data matrix itself as the dictionary (as done in [51, 52]). We thus tried the following two options: the first was to use the initial basis used for K-ALS and the second was to use the output basis learned by K-ALS. We found out that these two ways were comparable when we chose appropriate values for the regularization parameter λ. We thus only studied the first case. More precisely, we take the first $d' = 20$ vectors from each of the bases and form the dictionary by concatenating them in a matrix. Similarly to PCP, we address Gaussian noise by further applying the SSMS algorithm.

We fixed the parameters of K-ALS for all 105 images as follows: $\lambda_1 = \lambda_2 = \lambda_3 = \lambda_4 = 10^{-10}$, $n_1 = n_2 = 1$ and $n_3 = 5$ (see §4.2.1). For p, we tested both $p = p_0$ and $p = 2p_0$. We capped both PCP(capped) and K-PCP(capped) at 20. For PCP and K-PCP, the parameter λ was chosen to be 0.01 after testing the largest PSNR obtained among $\lambda = 10^k$, $k = -3, \ldots, 3$. Similarly, for PCP(capped)+SSMS and K-PCP(capped) the parameters (λ, γ) were chosen to be $(0.1, 0.001)$ after testing $(10^k, 10^l)$, $k, l = -3, \ldots, 3$. For LMaFit and K-LMaFit, we fine-tuned the best parameters based on PSNRs of the outputs. We first tested the following 7 values $\{10^k\}_{k=-3}^{3}$ and then searched around the best one in a finer scale until the results were not improved.

For the parameter λ in LRR, we first noticed that $\lambda = 10^{-3}$ obtained the best results among $\{10^k\}_{k=-3}^{3}$. To obtain even better results we tested the following 7 values in $[-3.5, -2.5]$: 0.0003, 0.0005, 0.0007, 0.001, 0.0015, 0.0022 and 0.0032. We chose $\lambda = 0.0015$ according to the best performance. As we explain below we only tested LRR for the 5 common images because it was too slow to run on the whole database.

6.2.3 Non-Local Medians

Many of the best performing image denoising methods (in the additive Gaussian noise setting) are versions of the non-local means algorithm (NLM) [66]. A standard version takes in parameters m, ϵ, and l, and defines a weight matrix $\mathbf{W}$ with elements

$$\mathbf{W}_{ij} = h(i)\, e^{-d(\mathbf{x}_i,\mathbf{x}_j)^2/\epsilon^2},$$

where $\mathbf{x}_i$ and $\mathbf{x}_j$ are patches of width $\sqrt{m}$ about pixels i and j respectively (represented as vectors in $\mathbb{R}^m$), h is 1 in a square neighborhood centered at i of sidelength l pixels and 0 elsewhere, and d denotes the Euclidean distance between the patches considered as vectors. A normalized weight $\tilde{\mathbf{W}}$ is formed by $\tilde{\mathbf{W}} = \mathbf{D}^{-1}(\mathbf{W} + \mathbf{W}^T)$, where $\mathbf{D}$ is the diagonal matrix with the row sums of $\mathbf{W} + \mathbf{W}^T$ on its diagonal. The noisy image is then smoothed by multiplying it with $\tilde{\mathbf{W}}$. The standard versions of NLM cannot handle impulsive noise or scratches, because the patch distance is too sensitive to outliers or gross corruptions.

We propose and test two robust versions of non-local means, which we refer to as the non-local medians. First, we define two different similarity functions between patches $\mathbf{x}_j$ and $\mathbf{x}_i$ (of width $\sqrt{m}$) as follows: 1) apply first a median filter to the entire image, and then use the regular Euclidean distance (d_2); 2) $\tilde{d}_r(\mathbf{x}_i - \mathbf{x}_j) := \sum_{k=1}^{m} \mu_k(\mathbf{x}_i(k) - \mathbf{x}_j(k))^2$, where $\mu_k = 1$ for the r coordinates of $\mathbf{x}_i - \mathbf{x}_j$ with smallest absolute difference $|\mathbf{x}_i - \mathbf{x}_j|$ and $\mu_k = 0$ on the other $m - r$ coordinates.

To find the non-local medians, we define a square neighborhood of length l for the i-th pixel and denote the indices of the pixels in this neighborhood by S_i. We compute the distances (d_2 after median filtering or $\tilde{d}_r$) between $\mathbf{x}_i$ and $\mathbf{x}_j$ for all $j \in S_i$. Then we form $\tilde{S}_i$ by keeping only s patches corresponding to the smallest distances. Finally, an estimate for the intensity value at pixel i is made by taking the median value among all intensities of pixels of patches in $\tilde{S}_i$. We refer to these two methods by NL-Median1 and NL-Median2 respectively.

In our experiments testing these two non-local medians methods, we let $m = 16$, $s = 12$, $l = 7$ and $r = \lfloor (1 - 2p_0)m \rfloor$. We remark that the algorithm is not sensitive to the choice of l as long as it is sufficiently large (but the algorithm slows as l gets larger). The parameter r was set to be adaptive to p_0. The other parameters were chosen by fine tuning numerical results.

We noticed that the application of SSMS after any of these methods does not in general help with reducing Gaussian noise. In fact, it tended to make things worse for small (or no) Gaussian noise and improved results for larger amounts, e.g., $\sigma \geq 20$ (though, this improvement with known σ and p_0 was still not better than K-ALS(p_0)).

6.2.4 Results

For each image, method and choice of corruption/denoising parameters, we averaged the PSNR over five simulations. Tables 6.4 and 6.5 report results of the different methods for denoising impulsive noise and blind inpainting respectively for the five popular images. We highlight the best results. Figures 6.8 and 6.9 plot the PSNR of the database of 100 images in several scenarios for denoising and inpainting respectively. The image IDs are sorted according to increasing PSNR of K-ALS($2p_0$) for better illustration.

The tables and figures omit some methods for the following reasons. The PCP algorithm is slow (as is evident from Table 6.3), we thus ran PCP+SSMS and K-PCP only for these five common images. Since MF+SSMS is similar to but better than MF+KSVD and since SSMS and K-SVD are designed only for Gaussian noise and thus not competitive at all, we only reported MF+SSMS among these. As for the non-local medians variants, which are described in §6.2.3, we report only NL-Median1 for blind inpainting and NL-Median2 for denoising since they are the best for these problems.

The PSNR of K-LMaFit was in the order of $25db$ and we thus did not report it in the tables. The reason for this poor performance is not clear to us since the distributed software of LMaFit at the time of submitting the paper is not open source. LRR gives good results on the 5 popular images, but it is slow; for example, it takes about a minute for K-ALS to finish the *House* image and several hours for LRR. We were thus unable to test it on the large database.

In addition to PSNR, we also evaluated the image quality by the Structural Similarity (SSIM) index [68]. For the five common images, SSIM for impulsive denoising is shown in Table 6.6 and for blind inpainting in Table 6.7. For the 100 images from the BSD database, SSIM is demonstrated in Figure 6.12 for denoising and Figure 6.13 for blind inpainting. We also report these results. We observe that the SSIM index favors K-ALS more than PSNR. The performance of PCP(capped)+SSMS in terms of SSIM oscillates much more, while it stays close to a certain level in terms of PSNR. Moreover,

we see that the performances of K-ALS(p_0) and K-ALS($2p_0$) are more correlated with each other when using SSIM than PSNR.

Besides PSNR and SSIM, we also demonstrate the visual quality of some denoising and blind inpainting results in Figures 6.10 and 6.11 respectively. The visual quality is important. Indeed, Figure 6.7 shows an image where PCP(capped)+SSMS obtains high values of both PSNR and SSIM for blind inpainting, but its visual output is clearly not satisfying.

Figure 6.7: Demonstration of the importance of visual quality. From left to right: Image corrupted by scratches only (no Gaussian noise or impulsive noise), outputs of NL-Median1 (PSNR=29.51, SSIM=0.8637), PCP(capped)+SSMS (PSNR=32.66, SSIM=0.9425) and ALS($2p_0$) (PSNR=31.70, SSIM=0.9425), where ALS($2p_0$) uses double of the true percentage of corruptions, while the other methods use the best values for their parameters among a fairly broad range. Although the PSNR and SSIM are high for the third image, its perceptual quality is not as good as the second and the fourth images. The second image is not as good as the fourth one due to unremoved scratches and over-smoothing.

We observe that PCP+SSMS and K-PCP are not practical because of long running times. Moreover, PCP+SSMS does not successfuly restore images in general and K-PCP (with additional thresholding) also fails in some cases, for example the image *House*. PCP(capped)+SSMS and K-PCP(capped) are fast but do not work well in general. LMaFit and K-LMaFit failed in general. The variants of the non-local medians cannot handle Gaussian noise well. The best of them is comparable to K-ALS when the Gaussian noise is low, but clearly worse as it increases. It is interesting to note that these variants are often effective with texture (even with noise), but do not perform well on smooth regions with noise. On the other hand, methods based on the median filter (e.g. MF+SSMS and IMF) tend to oversmooth the image and thus cannot handle textures well. For some blindly inpainted images PCP(capped) obtained high PSNR, but its perceptual quality was not good, that is, it was not able to remove many scratches.

Of all the methods we tested, LRR was the only one that could compete with K-ALS in terms of quality. However, it is very slow, costing two orders of magnitude more computation time. Even when significantly overestimating its main parameter p, K-ALS performs very well; in particular, it is good for various scenarios including texture, noisy smooth regions and scratches.

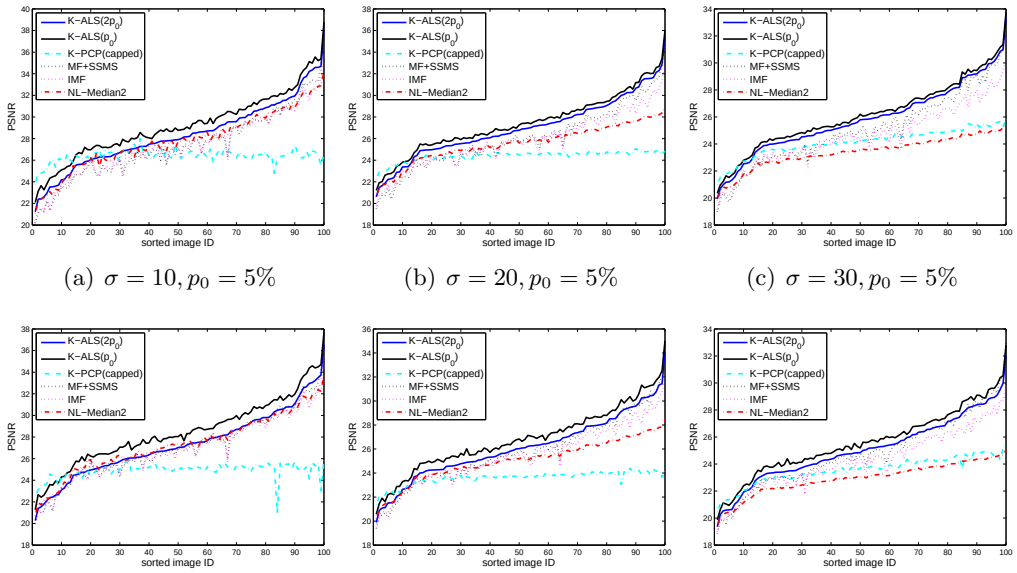

(a) $\sigma = 10, p_0 = 5\%$ (b) $\sigma = 20, p_0 = 5\%$ (c) $\sigma = 30, p_0 = 5\%$

(d) $\sigma = 10, p_0 = 10\%$ (e) $\sigma = 20, p_0 = 10\%$ (f) $\sigma = 30, p_0 = 10\%$

Figure 6.8: Performance (in PSNR) of denoising for the BSD database [64]. In each subfigure, PSNR of a specific corrupted scenario (see the subcaptions) is plotted versus the sorted image IDs. The number in the parenthesis after K-ALS specifies the input estimating the portion of corruptions. Other methods use the best values from a broad range of parameters, see 6.2.4. For most of the cases K-ALS outperforms the other algorithms, especially when the Gaussian noise is high.

6.2.5 Sensitivity of the K-ALS Algorithm w.r.t. the Dimension

In this section we study the sensitivity of the K-ALS algorithm w.r.t. the choice of the dimension d' in the two imaging problems. Intuitively, we observe that the SVD of the clusters of natural image patches can be well approximated with about rank 15 and slight overestimation cannot effect the results. Thus we tested K-ALS($2p_0$) on 2 of the popular images (*House* and *Lena*) with different values of d' (from 10 to 40) for both

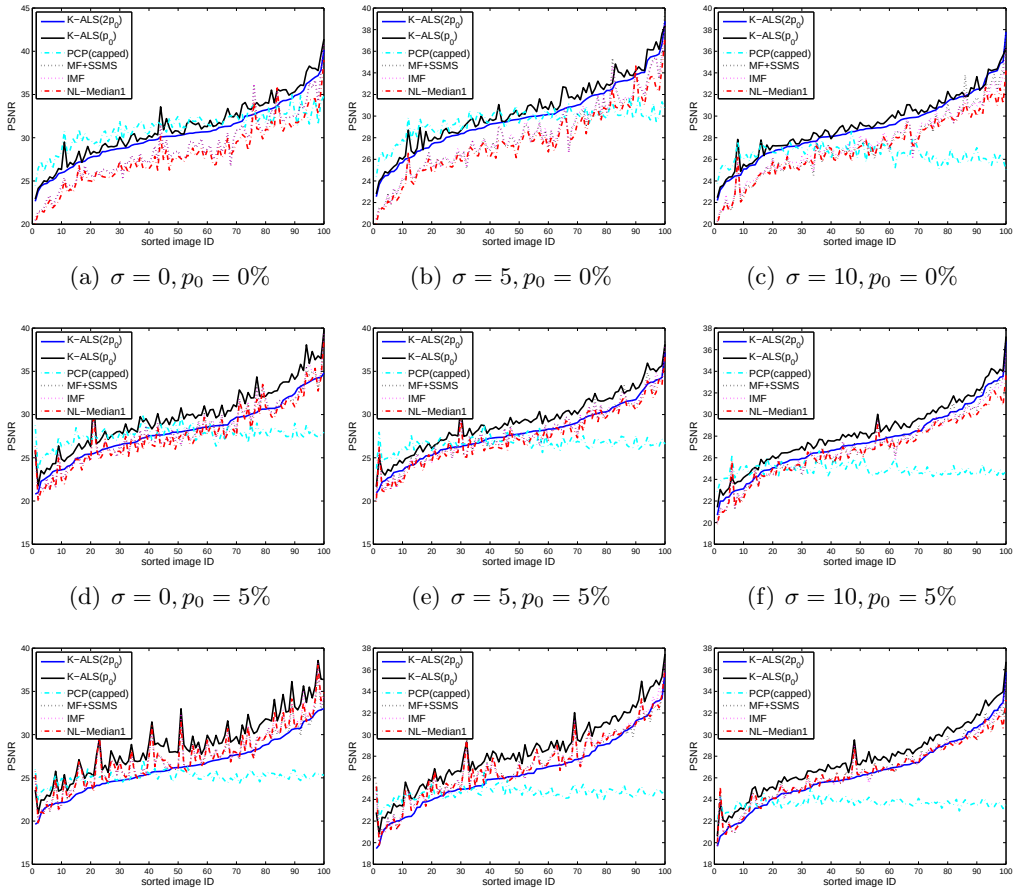

(a) $\sigma = 0, p_0 = 0\%$ (b) $\sigma = 5, p_0 = 0\%$ (c) $\sigma = 10, p_0 = 0\%$

(d) $\sigma = 0, p_0 = 5\%$ (e) $\sigma = 5, p_0 = 5\%$ (f) $\sigma = 10, p_0 = 5\%$

(g) $\sigma = 0, p_0 = 10\%$ (h) $\sigma = 5, p_0 = 10\%$ (i) $\sigma = 10, p_0 = 10\%$

Figure 6.9: Performance (in PSNR) of blind inpainting for the BSD database [64]. In each subfigure, PSNR of a specific corrupted scenario is plotted versus the sorted image IDs (the impulsive and Gaussian noise parameters are in the subcaptions and the scratch used throughout this paper is also added). The number in the parenthesis after K-ALS specifies the input estimating the portion of corruptions. Other methods use the best values from a broad range of parameters, see 6.2.4. In most cases K-ALS(p_0) outperforms other algorithms. However, K-ALS($2p_0$) is only advantageous with low-levels of corruption. For a few images the PSNR values of PCP(capped) are high, but their perceptual quality is not as satisfying.

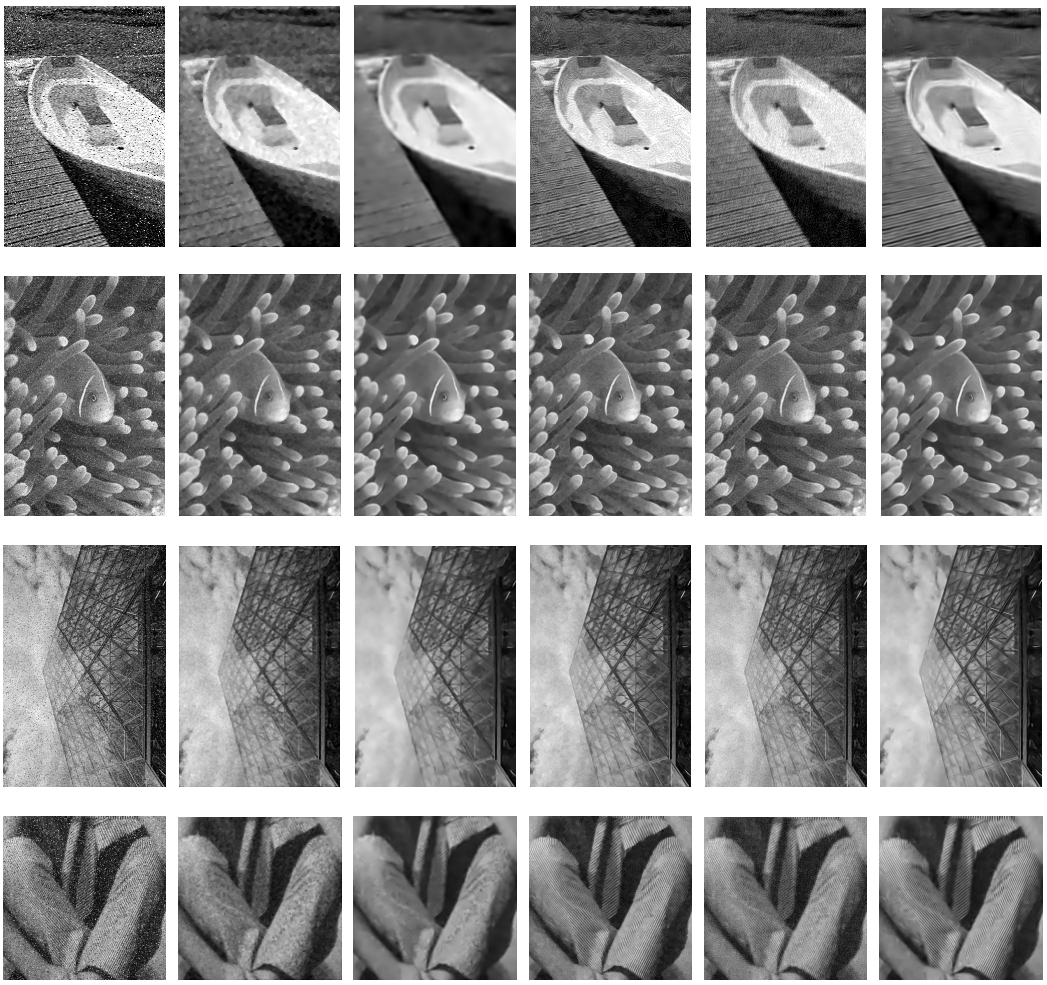

Figure 6.10: From left to right: noisy images, IMF, MF+SSMS, NL-Median2, K-PCP(capped) and K-ALS($2p_0$). The additive Gaussian noise has standard deviation $\sigma = 30$ for the first image and $\sigma = 20$ for the other three. The first three images have 5% impulsive noise and the last one has 10%. K-ALS, even with overestimated $p = 2p_0$ performs very well perceptually.

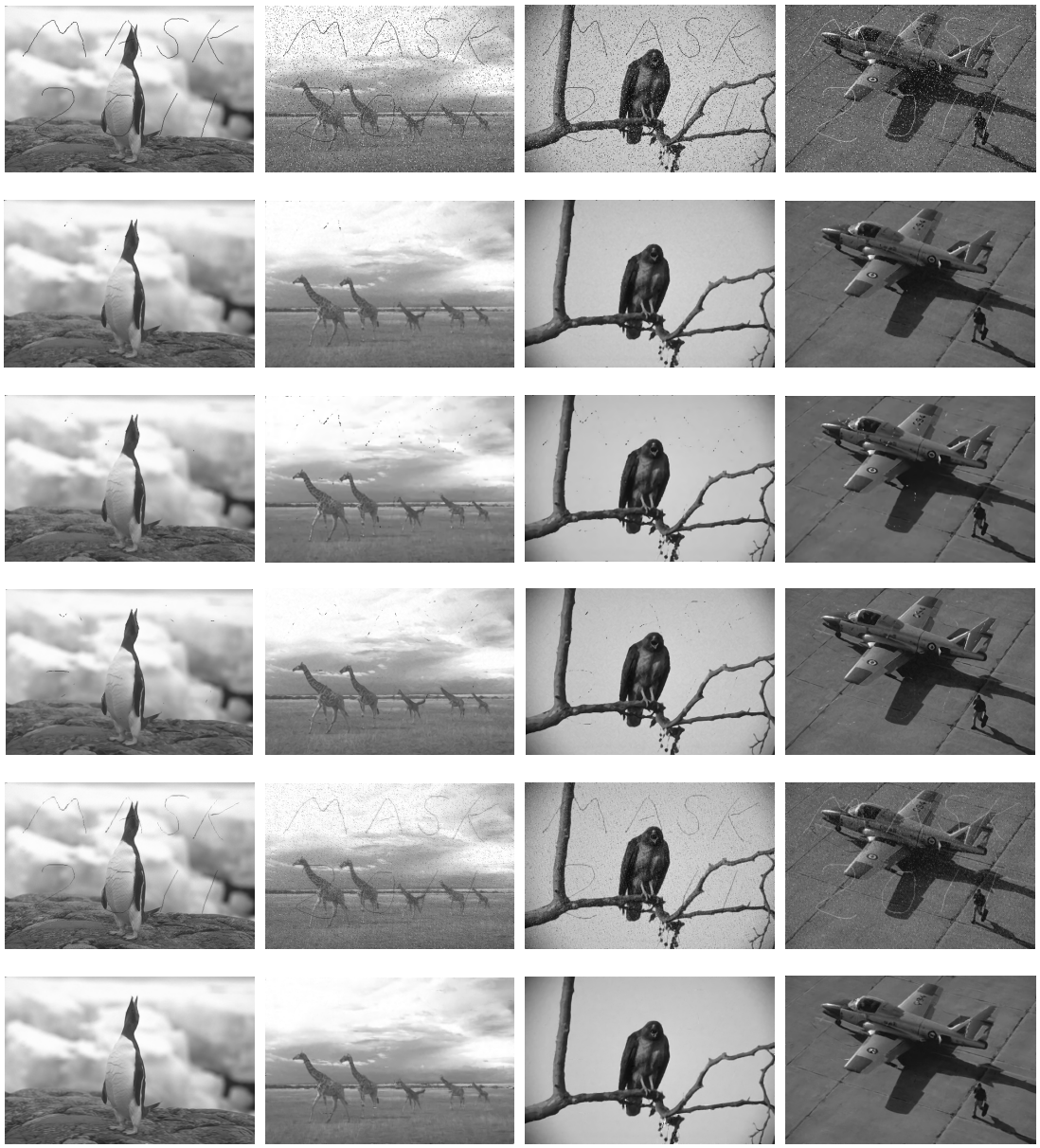

Figure 6.11: From top to bottom: corrupted images, IMF, MF+SSMS, NL-Median1, PCP(capped)+SSMS and K-ALS($2p_0$). The first image is only corrupted by scratches. The rest also have 5% impulsive noise and $\sigma = 10$ Gaussian noise. K-ALS, even with overestimated $p = 2p_0$, completely removes the scratches and still preserves image quality.

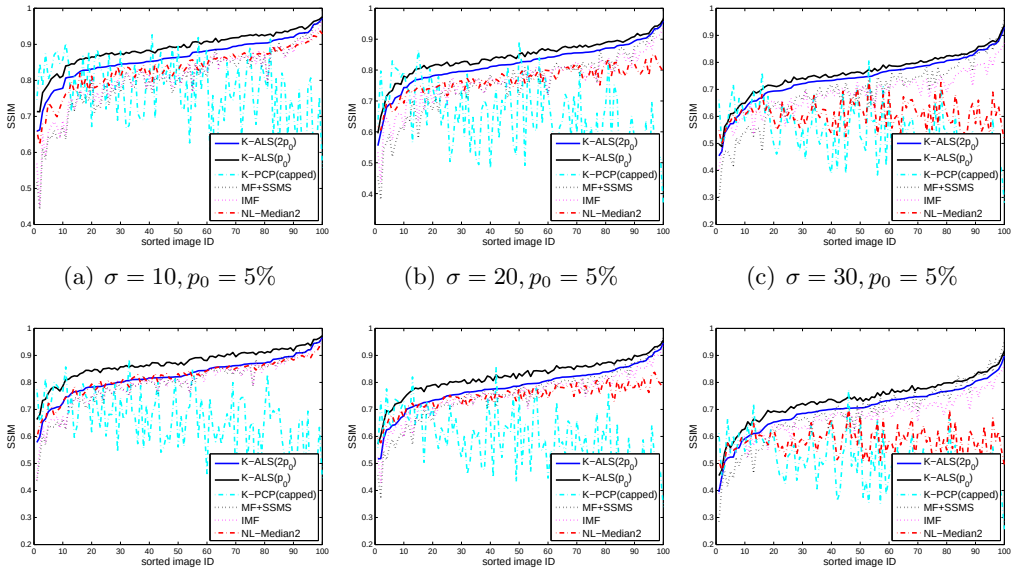

(a) $\sigma = 10, p_0 = 5\%$ (b) $\sigma = 20, p_0 = 5\%$ (c) $\sigma = 30, p_0 = 5\%$

(d) $\sigma = 10, p_0 = 10\%$ (e) $\sigma = 20, p_0 = 10\%$ (f) $\sigma = 30, p_0 = 10\%$

Figure 6.12: Performance (in SSIM) of denoising for the BSD database [64]. In each subfigure, SSIM of several approaches (see the legends) are plotted versus image ID for the case when the input image is corrupted by σ Gaussian noise and p_0 impulsive noise. K-ALS has the best performance for most of the cases, especially when the Gaussian noise is high.

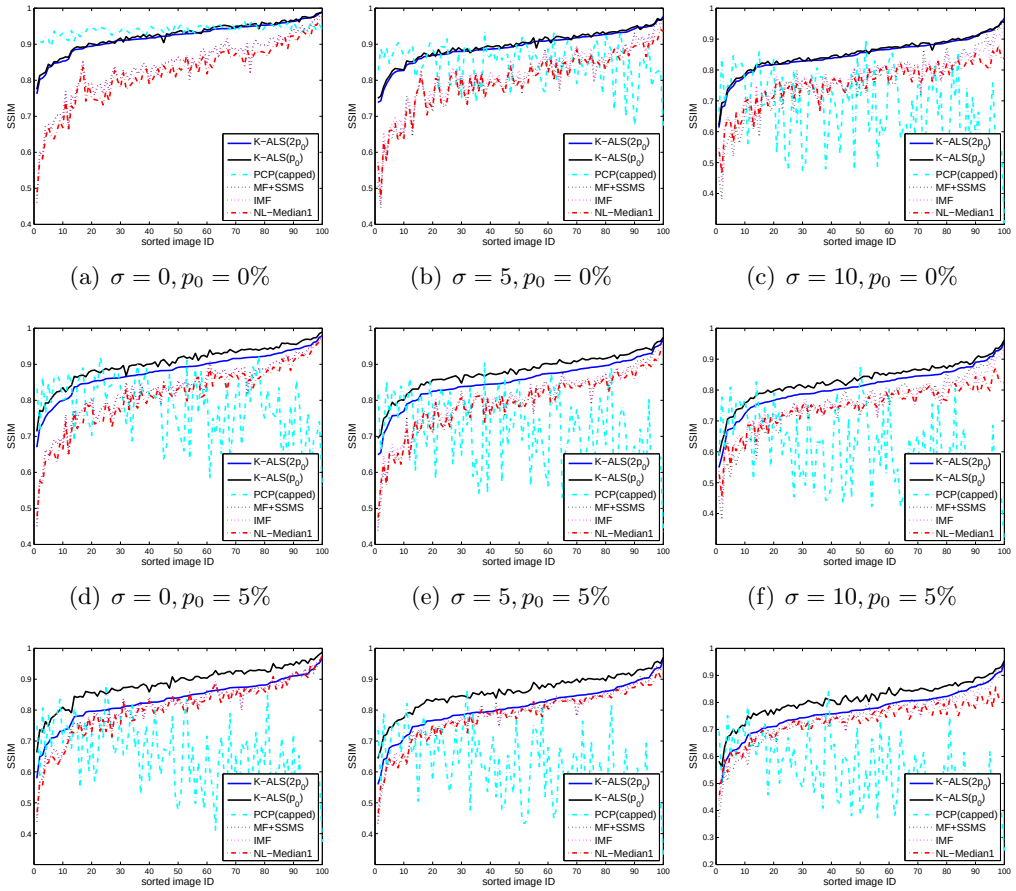

(a) $\sigma = 0, p_0 = 0\%$ (b) $\sigma = 5, p_0 = 0\%$ (c) $\sigma = 10, p_0 = 0\%$

(d) $\sigma = 0, p_0 = 5\%$ (e) $\sigma = 5, p_0 = 5\%$ (f) $\sigma = 10, p_0 = 5\%$

(g) $\sigma = 0, p_0 = 10\%$ (h) $\sigma = 5, p_0 = 10\%$ (i) $\sigma = 10, p_0 = 10\%$

Figure 6.13: Performance (in SSIM) of blind inpainting for the BSD database [64]. In each subfigure, SSIM of several approaches (see the legends) are plotted versus image ID for the case when the input image is corrupted by σ Gaussian noise, p_0 impulsive noise and some scratches. K-ALS has the best performance for most of the cases, especially when the Gaussian noise is high. For a few images the SSIM values of PCP(capped) are high, but their perceptual quality is not as satisfying.

denoising and blind inpainting. The results are shown in Figure 6.14, where in each subfigure performances (in PSNR) of different scenarios (with different p_0 and σ) are displayed. By these experiments, we conclude that K-ALS is robust to the choice of the dimension. It tends to improve with larger d' when the image is mildly corrupted, however, increasing d' could be worse if the image is largely degraded.

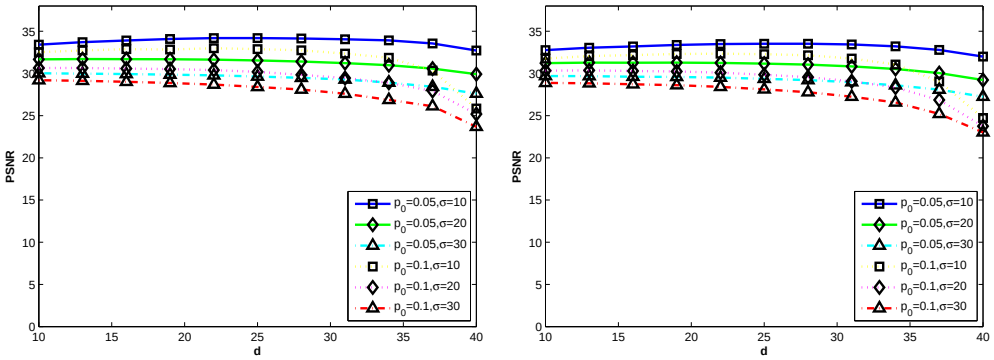

(a) denoising, *House* (b) denoising, *Lena*

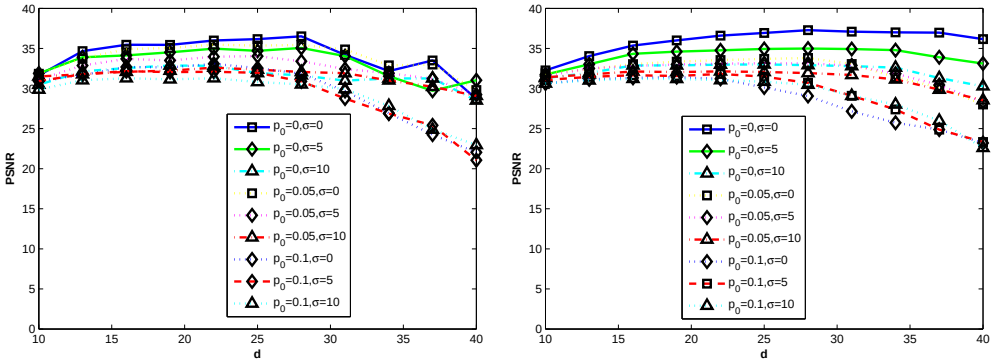

(c) blind inpainting, *House* (d) blind inpainting, *Lena*

Figure 6.14: The performance (in PSNR) of K-ALS($2p_0$) versus different values of the dimension d' for *House* (left) and *Lena* (right) for denoising (top) and blind inpainting (bottom). The different curves in the figures correspond to different values of σ and p_0 as specified. The K-ALS($2p_0$) is robust to the choice of d' and it favors small values for large corruptions and large values for small corruptions.

Table 6.4: Performance (in PSNR) of denoising for 5 popular images. Each row lists results of different approaches on a specific image corrupted by p_0 impulsive noise and Gaussian noise with standard deviation σ. The number in the parenthesis after K-ALS specifies the input parameter estimating the portion of corruptions. See Section 6.2.4 for details on the parameters used in all the algorithms. The best results are in bold. K-ALS and LRR outperform other methods for many of the cases; however, LRR is nearly two orders of magnitude slower than K-ALS.

		1	K-ALS($2p_0$)
		2	K-ALS(p_0)
		3	PCP(capped)+SSMS
		4	K-PCP(capped)
		5	KSVD
		6	SSMS
		7	MF+KSVD
		8	MF+SSMS
		9	IMF
		10	NL-Median2
		11	PCP+SSMS
		12	K-PCP
		13	LRR

	p_0	σ	1	2	3	4	5	6	7	8	9	10	11	12	13
Barbara	5%	10	30.77	**31.84**	26.35	26.61	22.06	22.81	24.74	24.96	24.63	29.73	24.11	29.18	31.59
		20	28.68	**29.22**	24.07	24.61	22.06	24.98	23.81	24.24	23.84	26.66	25.38	27.34	29.15
		30	26.99	**27.38**	23.56	24.55	23.16	26.22	22.93	23.67	23.05	23.96	26.19	25.67	27.38
	10%	10	29.30	**30.84**	24.34	25.31	19.26	19.59	24.59	24.77	24.35	29.20	19.77	28.45	28.35
		20	27.55	**28.64**	23.18	23.75	19.58	21.82	23.71	24.08	23.61	26.09	21.91	26.70	28.27
		30	25.99	26.63	22.99	23.93	21.00	23.85	22.81	23.52	22.89	23.47	23.96	25.20	**27.27**
Boat	5%	10	30.74	31.49	26.11	26.50	22.43	23.32	28.50	29.10	28.95	29.63	24.61	29.05	**31.71**
		20	28.88	**29.30**	24.51	24.55	22.54	25.46	26.55	27.46	27.06	26.69	25.94	27.43	29.15
		30	27.38	**27.69**	24.43	24.63	23.97	26.63	25.05	26.34	25.58	24.10	26.67	26.00	27.64
	10%	10	29.70	**30.84**	24.52	25.30	19.76	20.15	28.29	28.84	28.42	29.13	20.43	28.52	29.39
		20	27.99	**28.69**	23.74	23.79	20.55	22.55	26.39	27.23	26.69	26.21	22.67	26.98	27.86
		30	26.58	**27.09**	23.98	24.10	21.85	24.56	24.86	26.10	25.26	23.66	24.55	25.61	26.57
House	5%	10	34.15	**34.84**	26.11	28.15	22.42	23.51	31.85	32.16	31.09	31.85	33.90	28.26	28.52
		20	31.76	**32.17**	24.32	26.17	22.90	25.87	29.81	30.13	28.60	27.89	31.38	27.14	27.10
		30	29.79	**30.10**	24.80	26.43	24.92	28.11	27.24	28.81	26.93	24.81	30.23	25.99	25.88
	10%	10	32.96	**34.12**	24.75	26.66	19.75	20.25	31.27	31.52	30.42	31.41	28.75	27.74	28.17
		20	30.55	**31.32**	23.67	25.40	20.05	22.83	29.43	29.76	28.12	27.42	28.69	25.73	26.75
		30	28.82	**29.43**	24.35	25.71	22.34	25.55	26.93	28.38	26.47	24.35	28.16	25.61	25.54
Lena	5%	10	33.47	**34.19**	25.63	26.31	22.40	23.36	31.75	32.49	31.71	31.86	25.33	31.23	34.01
		20	31.29	**31.69**	23.92	24.53	22.76	25.62	29.28	30.40	29.17	27.81	26.36	29.39	31.31
		30	29.54	**29.85**	24.64	25.09	24.31	27.95	27.37	28.95	27.53	24.76	27.96	28.02	29.57
	10%	10	32.35	**33.49**	24.16	25.23	19.74	20.15	31.48	32.11	31.22	31.39	20.40	30.74	31.29
		20	30.20	**30.97**	23.39	23.85	20.01	22.61	29.07	30.11	28.82	27.34	22.56	28.96	29.52
		30	28.55	**29.15**	24.17	24.52	21.73	25.30	27.10	28.60	27.18	24.35	25.39	27.54	28.24
Peppers	5%	10	32.81	**33.44**	25.22	26.20	22.05	22.88	32.05	32.55	31.89	31.55	24.85	30.01	32.68
		20	31.01	**31.42**	24.16	24.54	22.32	24.94	30.03	30.64	29.53	27.71	25.87	28.75	30.95
		30	29.48	**29.82**	24.73	25.01	23.73	27.50	28.15	29.25	27.91	24.75	27.68	27.83	29.40
	10%	10	31.66	**32.81**	23.92	25.13	19.36	19.72	31.65	32.08	31.31	30.94	20.01	29.54	30.55
		20	29.88	**30.74**	23.40	23.78	19.57	21.96	29.69	30.24	29.10	27.20	21.99	28.37	29.15
		30	28.41	**29.07**	24.18	24.40	20.97	24.62	27.75	28.81	27.47	24.32	24.76	27.15	28.05

Table 6.5: Performance (in PSNR) of blind inpainting for 5 popular images. Each line lists results of different approaches on a specific image corrupted by σ Gaussian noise, p_0 impulsive noise and some scratches. The number in the parenthesis after K-ALS specifies the input parameter estimating the portion of corruptions. See Section 6.2.4 for details on the parameters used in all the algorithms. The best results are in bold. K-ALS and LRR outperform other methods for most images except *Peppers* which is relatively smooth (K-ALS results improve when we reduce the dimension and the number of subspaces); however, LRR is nearly two orders of magnitude slower than K-ALS

		1	K-ALS($2p_0$)
		2	K-ALS(p_0)
		3	PCP(capped)+SSMS
		4	K-PCP(capped)
		5	KSVD
		6	SSMS
		7	MF+KSVD
		8	MF+SSMS
		9	IMF
		10	NL-Median1
		11	PCP+SSMS
		12	K-PCP
		13	LRR

	p_0	σ	1	2	3	4	5	6	7	8	9	10	11	12	13
Barbara	0%	0	32.26	**32.97**	29.41	29.00	27.33	27.33	25.22	25.22	25.22	26.75	28.53	29.99	31.99
		5	31.32	**32.23**	28.49	28.31	27.09	27.10	25.15	25.23	25.06	26.60	27.95	29.25	31.09
		10	30.41	**30.90**	26.70	26.42	26.85	26.97	24.72	24.96	24.69	26.04	27.40	28.51	29.95
	5%	0	29.67	**31.60**	27.84	27.11	20.77	20.76	24.91	24.91	24.91	26.21	21.53	29.15	30.51
		5	29.30	**31.02**	27.23	26.68	20.96	21.00	24.90	24.99	24.77	26.05	21.72	28.56	30.06
		10	28.98	**29.97**	25.53	25.16	21.07	21.66	24.58	24.78	24.42	25.53	22.37	27.92	29.19
	10%	0	25.43	**30.45**	25.74	25.32	18.33	18.33	24.56	24.54	24.55	25.68	18.44	28.40	29.12
		5	26.05	**30.03**	25.34	25.12	18.44	18.43	24.62	24.70	24.46	25.53	18.53	27.93	28.93
		10	26.81	**28.95**	24.06	24.21	18.68	18.98	24.34	24.53	24.18	25.05	19.08	27.28	28.32
Boat	0%	0	30.67	32.80	29.76	28.63	26.96	26.96	30.31	30.31	30.31	29.54	28.88	30.65	**33.27**
		5	30.25	**31.84**	28.93	28.07	26.67	26.66	29.73	29.95	29.87	29.25	27.91	29.46	31.49
		10	29.59	**30.45**	26.48	26.15	26.40	26.51	28.41	29.01	28.89	28.57	27.08	28.58	30.17
	5%	0	29.66	31.65	27.59	26.93	21.06	21.05	29.74	29.72	29.72	29.24	21.92	29.37	**32.26**
		5	29.53	30.70	26.95	26.52	21.16	21.19	29.32	29.55	29.32	29.02	22.01	28.55	**31.01**
		10	28.92	29.65	25.32	25.01	21.35	21.98	28.14	28.72	28.41	28.26	22.69	28.00	**29.76**
	10%	0	28.00	30.88	25.57	25.42	18.66	18.66	28.84	28.94	28.95	28.90	18.83	28.75	**31.07**
		5	28.11	30.02	25.06	25.11	18.82	18.81	28.77	28.98	28.69	28.59	18.95	28.05	**30.25**
		10	27.99	**29.30**	23.94	24.11	19.08	19.42	27.74	28.31	28.00	27.92	19.63	27.50	29.09
House	0%	0	**36.44**	35.89	27.35	25.66	23.67	23.67	31.11	31.10	32.05	31.44	33.64	29.44	30.05
		5	**33.93**	33.63	27.02	25.49	23.66	23.66	30.89	31.05	31.57	30.37	31.38	29.10	29.28
		10	**32.19**	31.42	25.71	24.84	23.71	23.83	30.08	30.52	30.54	29.51	29.63	28.38	28.55
	5%	0	35.41	**36.58**	26.38	24.65	20.00	20.00	29.98	29.98	31.40	30.81	28.95	28.39	29.53
		5	33.29	**33.90**	25.81	24.62	20.08	20.12	29.99	30.06	30.92	30.14	27.59	28.52	28.84
		10	31.79	**31.54**	24.54	24.26	20.35	20.89	29.16	29.75	30.00	29.03	27.15	28.21	28.24
	10%	0	32.67	**35.80**	24.58	23.63	18.02	18.02	28.43	28.53	30.48	30.19	22.67	27.93	29.19
		5	32.15	**33.67**	24.26	23.69	18.16	18.16	28.94	28.74	30.23	29.71	22.36	28.85	28.39
		10	31.20	**32.23**	23.60	23.56	18.47	18.80	28.60	28.70	29.39	28.54	23.16	27.94	27.92
Lena	0%	0	35.32	**36.65**	30.94	29.23	27.72	27.72	34.38	34.38	34.38	33.11	30.90	32.81	36.48
		5	34.15	**34.97**	29.72	28.69	27.49	27.50	33.24	33.54	33.33	32.64	29.73	31.76	34.36
		10	32.84	**33.03**	26.26	26.62	27.36	27.47	31.49	32.29	31.70	31.30	28.75	30.82	32.88
	5%	0	33.71	**35.46**	27.99	27.00	21.19	21.19	33.50	33.44	33.44	32.78	22.46	31.71	35.31
		5	33.10	**34.29**	26.87	26.94	21.37	21.43	32.73	32.94	32.55	32.33	22.54	30.94	33.81
		10	32.15	**32.77**	24.80	25.39	21.45	22.12	31.14	31.89	31.28	30.90	23.23	30.25	32.43
	10%	0	31.24	**34.81**	25.45	25.55	18.72	18.72	32.00	32.18	32.56	32.44	18.90	31.15	34.20
		5	31.73	**33.61**	24.92	25.57	18.84	18.85	31.91	32.19	32.02	31.93	19.05	30.50	33.09
		10	31.17	**32.22**	23.76	24.45	19.17	19.51	30.57	31.29	30.75	30.49	19.75	29.75	31.69
Peppers	0%	0	29.22	31.26	31.36	29.23	27.68	27.67	**34.22**	**34.22**	**34.22**	32.93	30.97	32.08	32.58
		5	28.66	30.24	29.19	28.68	27.38	27.37	33.22	**33.46**	33.34	32.58	29.78	30.98	31.51
		10	29.50	30.85	27.62	26.80	20.93	20.93	31.89	**32.40**	32.00	31.28	28.74	30.23	31.12
	5%	0	29.50	30.85	27.62	26.80	20.93	20.93	33.31	33.25	**33.45**	32.48	22.21	31.31	32.08
		5	29.07	30.64	26.49	26.85	21.04	21.09	32.68	**32.89**	32.80	32.07	22.42	30.37	31.34
		10	29.09	30.40	24.60	25.38	21.16	21.74	31.45	**31.92**	31.50	30.79	23.02	29.75	30.86
	10%	0	28.54	31.09	25.12	25.32	18.43	18.42	31.85	31.99	**32.69**	32.12	18.69	30.65	31.41
		5	29.07	30.14	24.60	25.35	18.55	18.55	31.74	31.96	**32.17**	31.62	18.69	29.86	30.98
		10	28.70	29.98	23.62	24.40	18.80	19.11	30.74	**31.26**	30.95	30.37	19.36	29.14	30.40

Table 6.6: Performance (in SSIM) of denoising for 5 popular images. Each line lists results of different approaches on a specific image corrupted by σ Gaussian noise and p_0 impulsive noise. The best results are in bold. K-ALS outperforms other methods for most images except *Peppers*.

1	K-ALS($2p_0$)	
2	K-ALS(p_0)	
3	PCP(capped)+SSMS	
4	K-PCP(capped)	
5	KSVD	
6	SSMS	
7	MF+KSVD	
8	MF+SSMS	
9	IMF	
10	NL-Median2	
11	PCP+SSMS	
12	K-PCP	
13	LRR	

	p_0	σ	1	2	3	4	5	6	7	8	9	10	11	12	13
Barbara	5%	10	0.897	**0.912**	0.654	0.656	0.582	0.616	0.726	0.754	0.727	0.846	0.641	0.874	0.895
		20	0.836	**0.849**	0.538	0.557	0.578	0.672	0.654	0.692	0.642	0.679	0.681	0.812	0.827
		30	0.777	**0.791**	0.509	0.554	0.625	0.710	0.604	0.653	0.595	0.535	0.708	0.750	0.768
	10%	10	0.867	**0.896**	0.566	0.607	0.425	0.442	0.723	0.749	0.717	0.832	0.444	0.859	0.875
		20	0.799	**0.826**	0.485	0.521	0.421	0.516	0.651	0.686	0.634	0.655	0.517	0.797	0.806
		30	0.733	**0.763**	0.473	0.529	0.495	0.600	0.601	0.648	0.586	0.509	0.603	0.739	0.748
Boat	5%	10	0.839	**0.854**	0.610	0.618	0.525	0.571	0.750	0.792	0.787	0.794	0.601	0.807	0.844
		20	0.770	**0.783**	0.496	0.500	0.523	0.633	0.673	0.727	0.700	0.619	0.640	0.742	0.772
		30	0.715	**0.727**	0.489	0.496	0.581	0.663	0.622	0.682	0.641	0.473	0.662	0.688	0.714
	10%	10	0.812	**0.841**	0.529	0.565	0.383	0.404	0.746	0.787	0.777	0.777	0.404	0.795	0.833
		20	0.740	**0.765**	0.465	0.464	0.368	0.485	0.668	0.723	0.690	0.596	0.491	0.728	0.760
		30	0.679	**0.704**	0.472	0.471	0.461	0.567	0.618	0.678	0.630	0.448	0.572	0.679	**0.704**
House	5%	10	0.878	**0.888**	0.508	0.600	0.482	0.537	0.848	0.856	0.834	0.804	0.874	0.821	0.815
		20	0.836	**0.844**	0.410	0.497	0.519	0.604	0.812	0.824	0.776	0.598	0.816	0.794	0.783
		30	0.797	**0.805**	0.435	0.527	0.612	0.684	0.759	0.800	0.712	0.442	0.790	0.767	0.752
	10%	10	0.861	**0.879**	0.452	0.547	0.323	0.350	0.845	0.853	0.792	0.790	0.681	0.816	0.811
		20	0.810	**0.828**	0.391	0.469	0.338	0.447	0.811	0.821	0.767	0.578	0.715	0.794	0.775
		30	0.765	0.784	0.416	0.498	0.449	0.559	0.761	**0.794**	0.702	0.422	0.698	0.777	0.747
Lena	5%	10	0.884	**0.894**	0.498	0.530	0.477	0.531	0.849	0.871	0.846	0.811	0.574	0.868	0.890
		20	0.837	**0.847**	0.402	0.429	0.516	0.616	0.799	0.831	0.781	0.603	0.632	0.826	0.846
		30	0.794	0.805	0.427	0.451	0.605	0.700	0.759	0.800	0.719	0.442	0.703	0.793	**0.810**
	10%	10	0.864	**0.884**	0.433	0.485	0.318	0.342	0.848	0.868	0.839	0.796	0.351	0.863	0.881
		20	0.808	0.828	0.383	0.400	0.337	0.447	0.797	0.828	0.773	0.582	0.441	0.819	**0.833**
		30	0.758	0.781	0.414	0.428	0.441	0.576	0.755	0.795	0.709	0.422	0.578	0.784	**0.796**
Peppers	5%	10	0.850	**0.860**	0.479	0.523	0.453	0.503	0.834	0.847	0.830	0.794	0.549	0.838	0.856
		20	0.812	0.822	0.401	0.425	0.488	0.578	0.802	0.818	0.776	0.596	0.600	0.810	**0.823**
		30	0.776	0.786	0.437	0.444	0.575	0.673	0.771	0.792	0.715	0.439	0.676	0.783	**0.795**
	10%	10	0.833	**0.851**	0.425	0.478	0.302	0.324	0.831	0.844	0.825	0.780	0.332	0.834	0.848
		20	0.780	0.802	0.380	0.391	0.313	0.416	0.798	**0.813**	0.768	0.575	0.414	0.803	0.810
		30	0.740	0.763	0.417	0.422	0.407	0.538	0.766	**0.787**	0.706	0.419	0.546	0.777	0.781

Table 6.7: Performance (in SSIM) of blind inpainting for 5 popular images. Each line lists results of different approaches on a specific image corrupted by σ Gaussian noise, p_0 impulsive noise and some scratches. The best results are in bold. We note that for most cases K-ALS outperforms other methods.

		1	K-ALS($2p_0$)
		2	K-ALS(p_0)
		3	PCP(capped)+SSMS
		4	K-PCP(capped)
		5	KSVD
		6	SSMS
		7	MF+KSVD
		8	MF+SSMS
		9	IMF
		10	NL-Median1
		11	PCP+SSMS
		12	K-PCP
		13	LRR

	p_0	σ	1	2	3	4	5	6	7	8	9	10	11	12	13
Barbara	0%	0	0.956	0.959	0.938	0.944	0.945	0.945	0.809	0.809	0.809	0.860	0.949	0.937	**0.960**
		5	0.932	**0.936**	0.873	0.891	0.912	0.911	0.780	0.789	0.784	0.839	0.915	0.898	0.921
		10	0.904	**0.908**	0.730	0.717	0.886	0.887	0.725	0.755	0.732	0.788	0.888	0.866	0.890
	5%	0	0.936	**0.950**	0.851	0.808	0.564	0.5664	0.798	0.798	0.798	0.846	0.587	0.920	0.935
		5	0.913	**0.927**	0.791	0.765	0.562	0.567	0.773	0.782	0.772	0.824	0.583	0.883	0.907
		10	0.882	**0.895**	0.657	0.644	0.557	0.589	0.721	0.749	0.722	0.770	0.610	0.851	0.877
	10%	0	0.863	**0.938**	0.710	0.690	0.408	0.407	0.784	0.784	0.784	0.831	0.406	0.903	0.893
		5	0.848	**0.914**	0.670	0.667	0.406	0.407	0.764	0.772	0.756	0.807	0.407	0.868	0.879
		10	0.830	**0.877**	0.574	0.594	0.406	0.423	0.715	0.741	0.711	0.751	0.431	0.837	0.852
Boat	0%	0	0.920	0.930	0.930	0.921	0.932	0.932	0.847	0.847	0.847	0.851	0.941	0.929	**0.959**
		5	0.884	**0.894**	0.853	0.853	0.878	0.871	0.812	0.830	0.825	0.832	0.877	0.852	0.883
		10	0.843	**0.851**	0.664	0.673	0.826	0.826	0.748	0.791	0.789	0.787	0.828	0.809	0.837
	5%	0	0.900	0.918	0.793	0.784	0.538	0.538	0.838	0.838	0.838	0.845	0.566	0.902	**0.937**
		5	0.864	**0.882**	0.730	0.737	0.526	0.528	0.808	0.824	0.818	0.825	0.553	0.831	0.876
		10	0.821	**0.837**	0.598	0.602	0.508	0.548	0.744	0.786	0.781	0.776	0.572	0.792	0.829
	10%	0	0.862	**0.907**	0.656	0.665	0.369	0.369	0.824	0.824	0.827	0.837	0.372	0.886	0.902
		5	0.829	**0.868**	0.613	0.635	0.369	0.369	0.800	0.815	0.810	0.814	0.371	0.821	0.860
		10	0.790	**0.824**	0.520	0.548	0.367	0.386	0.737	0.779	0.770	0.764	0.390	0.777	0.813
House	0%	0	**0.955**	0.954	0.866	0.855	0.849	0.849	0.868	0.868	0.883	0.881	0.929	0.899	0.894
		5	0.914	**0.915**	0.775	0.810	0.809	0.805	0852	0.860	0.865	0.846	0.867	0.856	0.839
		10	**0.870**	0.866	0.567	0.629	0.767	0.770	0.831	0.841	0.831	0.788	0.817	0.815	0.815
	5%	0	0.953	**0.961**	0.703	0.692	0.457	0.457	0.854	0.855	0.877	0.872	0.755	0.871	0.883
		5	0.907	**0.915**	0.614	0.677	0.438	0.443	0.845	0.848	0.858	0.841	0.744	0.837	0.834
		10	0.863	**0.867**	0.480	0.563	0.435	0.474	0.820	0.831	0.826	0.776	0.740	0.809	0.811
	10%	0	0.925	**0.956**	0.540	0.566	0.300	0.300	0.829	0.833	0.867	0.867	0.454	0.861	0.874
		5	0.881	**0.910**	0.498	0.564	0.295	0.297	0.829	0.831	0.848	0.832	0.435	0.839	0.827
		10	0.844	**0.862**	0.433	0.510	0.301	0.323	0.812	0.818	0.819	0.766	0.504	0.809	0.806
Lena	0%	0	0.950	0.955	0.932	0.924	0.933	0.933	0.918	0.918	0.918	0.909	0.943	0.940	**0.970**
		5	0.916	**0.921**	0.809	0.837	0.883	0.880	0.883	0.894	0.889	0.885	0.888	0.887	0.911
		10	0.886	**0.888**	0.549	0.590	0.851	0.852	0.846	0.869	0.847	0.829	0.856	0.861	0.881
	5%	0	0.936	0.949	0.722	0.710	0.480	0.480	0.909	0.910	0.910	0.905	0.513	0.916	**0.954**
		5	0.903	**0.914**	0.629	0.672	0.469	0.476	0.879	0.889	0.884	0.880	0.512	0.874	0.906
		10	0.872	**0.881**	0.474	0.518	0.458	0.501	0.843	0.865	0.841	0.818	0.540	0.850	0.875
	10%	0	0.907	**0.942**	0.553	0.582	0.305	0.305	0.897	0.897	0.900	0.900	0.306	0.908	0.930
		5	0.883	**0.906**	0.510	0.563	0.302	0.304	0.872	0.882	0.878	0.872	0.308	0.867	0.894
		10	0.851	**0.871**	0.428	0.471	0.308	0.329	0.837	0.859	0.833	0.806	0.335	0.842	0.861
Peppers	0%	0	0.928	0.924	0.912	0.920	0.928	0.928	0.886	0.886	0.886	0.875	0.938	0.916	**0.959**
		5	**0.878**	0.875	0.753	0.810	0.860	0.851	0.856	0.864	0.866	0.855	0.860	0.849	0.875
		10	**0.847**	0.846	0.512	0.571	0.818	0.818	0.832	0.846	0.831	0.803	0.822	0.827	**0.847**
	5%	0	0.916	0.925	0.689	0.688	0.466	0.466	0.878	0.878	0.879	0.872	0.497	0.911	**0.941**
		5	0.869	**0.877**	0.603	0.657	0.449	0.452	0.852	0.860	0.861	0.849	0.491	0.844	0.872
		10	0.840	**0.844**	0.465	0.507	0.437	0.477	0.828	0.841	0.826	0.793	0.514	0.823	0.842
	10%	0	0.889	**0.919**	0.533	0.561	0.291	0.291	0.865	0.866	0.874	0.868	0.296	0.903	0.911
		5	0.852	**0.872**	0.493	0.547	0.290	0.290	0.844	0.852	0.855	0.843	0.288	0.837	0.862
		10	0.821	**0.836**	0.419	0.462	0.288	0.307	0.821	0.834	0.820	0.782	0.313	0.816	0.831

Chapter 7

Conclusion and Discussion

7.1 Conclusions

This manuscript has suggested automatic ways to determine the dimension and number of subspaces in HLM. We have provided an efficient way to quantitatively implement elbow heuristic. This method allows us to find the number of subspaces given the dimension or find the dimension and number of subspaces simultaneously. We have also suggested a method to locally estimate the dimension, which can be used combined with the elbow method. Some extensive simulations have been performed to compare our algorithms with some other standard methods. We have also applied our methods to real data. It seems that our methods obtain satisfactory results with much less computing complexity. We have done some theoretical computation for simple continuous cases, which supports our algorithms.

Furthermore, we have shown that localized versions of robust PCA are sometimes necessary and sufficient to model corrupted data which has local (but not global) low dimensional structure. In particular, we see that the problems of denoising images with impulsive noise and blind inpainting can be approached via localized robust PCA methods. For these problems we have shown that a robust PCA algorithm, which is based on an alternating least square approach, performs very well. We have also established a convergence result for the proposed procedure. There is still much to do. In particular, there is almost no theory for when recovery is possible with a manifold model; we suspect that it may be possible to construct a theory analogous to that of

[69].

The manuscript also suggests some interesting future work as follows:

- Detection of non-structural data. Our work assumes that the data is structured and is not able to find $K_{\mathrm{SOD}} = 1$. However, it's meaningful to determine whether the data is clustered in real cases. We are interested in modifying the current elbow method such that it's good for $K = 1$.

- Determination of mixed dimensions. Our work also assumes that the subspaces have the same dimension. However, subspaces are often of different dimensions in real data. We would like to figure out a way to find the mixed dimensions.

- Further theoretical analysis. We showed some examples in continuous case. Further theoretical analysis will make the method more rigorous and clear.

References

[1] Y. Ma, A. Y. Yang, H. Derksen, and R. Fossum. Estimation of subspace arrangements with applications in modeling and segmenting mixed data. *SIAM Review*, 50(3):413–458, 2008.

[2] R. Vidal, Y. Ma, and S. Sastry. Generalized principal component analysis (GPCA). *IEEE Transactions on Pattern Analysis and Machine Intelligence*, 27(12), 2005.

[3] Y. Ma, H. Derksen, W. Hong, and J. Wright. Segmentation of multivariate mixed data via lossy coding and compression. *IEEE Transactions on Pattern Analysis and Machine Intelligence*, 29(9):1546–1562, September 2007.

[4] Robert Tibshirani and Guenther Walther. Estimating the number of clusters in a dataset via the gap statistic. *Journal of the Royal Statistical Society B*, 63,Part 2:411–423, 2001.

[5] D. Pelleg and A. Moore. X-means: Extending K-means with efficient estimation of the number of clusters. In *Proc. 17th International Conf. on Machine Learning*, pages 727–734. Morgan Kaufmann, San Francisco, CA, 2000.

[6] L. Zelnik-Manor and P. Perona. Self-tuning spectral clustering. In *Advances in Neural Information Processing Systems 17*, pages 1601–1608, 2004.

[7] Shihong Yue, Xiuxiu Wang, and Miaomiao Wei. Application of two-order difference to gap statistic. *Transactions of Tianjin University*, 14:217–221, 2008. 10.1007/s12209-008-0039-1.

[8] Bin Dong, Hui Ji, Jia Li, Zuowei Shen, and Yuhong Xu. Wavelet frame based blind image inpainting. *Applied and Computational Harmonic Analysis*, 32(2):268–279, 2011.

[9] Ming Yan. Restoration of images corrupted by impulse noise using blind inpainting and l_0 norm. Technical Report CAM report 11-72, Department of Mathematics, University of California, Los Angeles.

[10] M. Elad and M. Aharon. Image denoising via learned dictionaries and sparse representation. In *In CVPR*, pages 17–22, 2006.

[11] G. Yu, G. Sapiro, and S. Mallat. Image modeling and enhancement via structured sparse model selection. In *IEEE International Conference on Image Processing (ICIP)*, 2010.

[12] N. Kambhatla and T. K. Leen. Fast non-linear dimension reduction. In *Advances in Neural Information Processing Systems 6*, pages 152–159. Morgan Kaufmann, 1994.

[13] P. Bradley and O. Mangasarian. k-plane clustering. *J. Global optim.*, 16(1):23–32, 2000.

[14] P. Tseng. Nearest q-flat to m points. *Journal of Optimization Theory and Applications*, 105:249–252, 2000. 10.1023/A:1004678431677.

[15] J. Ho, M. Yang, J. Lim, K. Lee, and D. Kriegman. Clustering appearances of objects under varying illumination conditions. In *Proceedings of International Conference on Computer Vision and Pattern Recognition*, volume 1, pages 11–18, 2003.

[16] V. Chandrasekaran, S. Sanghavi, P. A. Parrilo, and A. S. Willsky. Rank-sparsity incoherence for matrix decomposition. *Arxiv*, 02139:1–24, 2009.

[17] E. J. Candès, X. Li, Y. Ma, and J. Wright. Robust principal component analysis? *J. ACM*, 58(3):11, 2011.

[18] Y. Shen, Z. Wen, and Y. Zhang. Augmented lagrangian alternating direction method for matrix separation based on low-rank factorization. Technical Report TR11-02, Rice University, January 2011.

[19] J. Costeira and T. Kanade. A multibody factorization method for independently moving objects. *International Journal of Computer Vision*, 29(3):159–179, 1998.

[20] P. H. S. Torr. Geometric motion segmentation and model selection. *Phil. Trans. Royal Society of London A*, 356:1321–1340, 1998.

[21] M. Tipping and C. Bishop. Mixtures of probabilistic principal component analysers. *Neural Computation*, 11(2):443–482, 1999.

[22] K. Kanatani. Motion segmentation by subspace separation and model selection. In *Proc. of 8th ICCV*, volume 3, pages 586–591. Vancouver, Canada, 2001.

[23] K. Kanatani. Evaluation and selection of models for motion segmentation. In *7th ECCV*, volume 3, pages 335–349, May 2002.

[24] J. Yan and M. Pollefeys. A general framework for motion segmentation: Independent, articulated, rigid, non-rigid, degenerate and nondegenerate. In *ECCV*, volume 4, pages 94–106, 2006.

[25] A. Y. Yang, S. R. Rao, and Y. Ma. Robust statistical estimation and segmentation of multiple subspaces. In *CVPRW '06: Proceedings of the 2006 Conference on Computer Vision and Pattern Recognition Workshop*, page 99, Washington, DC, USA, 2006. IEEE Computer Society.

[26] G. Chen and G. Lerman. Spectral curvature clustering (SCC). *Int. J. Comput. Vision*, 81(3):317–330, 2009.

[27] Akram Aldroubi, Carlos Cabrelli, and Ursula Molter. Optimal non-linear models for sparsity and sampling. *Journal of Fourier Analysis and Applications*, 14(5-6):793–812, December 2008.

[28] T. Zhang, A. Szlam, and G. Lerman. Median K-flats for hybrid linear modeling with many outliers. In *Computer Vision Workshops (ICCV Workshops), 2009 IEEE 12th International Conference on Computer Vision*, pages 234–241, Kyoto, Japan, 2009.

[29] T. Zhang, A. Szlam, Y. Wang, and G. Lerman. Randomized hybrid linear modeling by local best-fit flats. In *Computer Vision and Pattern Recognition (CVPR), 2010 IEEE Conference on*, pages 1927 –1934, jun. 2010.

[30] C. R. Vogel. Non-convergence of the L-curve regularization parameter selection method. *Inverse Problems*, 12:535–547, August 1996.

[31] G. Lerman and J. T. Whitehouse. On d-dimensional semimetrics and simplex-type inequalities for high-dimensional sine functions. *Journal of Approximation Theory*, 156(1):52–81, 2009.

[32] E. Levina and P. J. Bickel. Maximum likelihood estimation of intrinsic dimension. In Lawrence K. Saul, Yair Weiss, and Léon Bottou, editors, *Advances in Neural Information Processing Systems 17*, pages 777–784. MIT Press, Cambridge, MA, 2005.

[33] M. Hein, J. Audibert, and U. von Luxburg. From graphs to manifolds - weak and strong pointwise consistency of graph laplacians. In *Proceedings of the 18th Conference on Learning Theory (COLT)*, pages 470–485, 2005.

[34] K. Fukunaga and D. R. Olsen. An algorithm for finding intrinsic dimensionality of data. *IEEE Trans. Comput.*, 20(2):176–183, 1971.

[35] P. J. Huber. *Robust Statistics*. John Wiley & Sons Inc., New York, 1981. Wiley Series in Probability and Mathematical Statistics.

[36] R. A. Maronna, R. D. Martin, and V. J. Yohai. *Robust statistics: Theory and methods*. Wiley Series in Probability and Statistics. John Wiley & Sons Ltd., Chichester, 2006.

[37] D. Hsu, S.M. Kakade, and Tong Zhang. Robust matrix decomposition with sparse corruptions. *Information Theory, IEEE Transactions on*, 57(11):7221 –7234, nov. 2011.

[38] Z. Lin, A. Ganesh, J. Wright, L. Wu, M. Chen, and Y. Ma. Fast convex optimization algorithms for exact recovery of a corrupted low-rank matrix. preprint, July 2009.

[39] A. E. Waters, A. C. Sankaranarayanan, and R. G. Baraniuk. Sparcs: Recovering low-rank and sparse matrices from compressive measurements. In *Neural Information Processing Systems (NIPS)*, Granada, Spain, Dec. 2011.

[40] Z. Zhou, X. Li, J. Wright, E. J. Candès, and Y. Ma. Stable principal component pursuit. *CoRR*, abs/1001.2363, 2010.

[41] A. Agarwal, S. Negahban, and M. Wainwright. Noisy matrix decomposition via convex relaxation: Optimal rates in high dimensions. In Lise Getoor and Tobias Scheffer, editors, *Proceedings of the 28th International Conference on Machine Learning (ICML-11)*, ICML '11, pages 1129–1136, New York, NY, USA, June 2011. ACM. extended version at http://arxiv.org/abs/1102.4807.

[42] Min Tao and Xiaoming Yuan. Recovering low-rank and sparse components of matrices from incomplete and noisy observations. *SIAM Journal on Optimization*, 21(1):57–81, 2011.

[43] T. Wiberg. Computation of principal components when data are missing. *Proc 2nd Symposium on Computational Statistics Berlin Germany*, pages 229–326, 1976.

[44] B. Triggs, P. F. McLauchlan, R. I. Hartley, and A. W. Fitzgibbon. Bundle adjustment - a modern synthesis. In *Proceedings of the International Workshop on Vision Algorithms: Theory and Practice*, ICCV '99, pages 298–372, London, UK, 2000. Springer-Verlag.

[45] R. Vidal and R. I. Hartley. Motion segmentation with missing data using powerfactorization and gpca. In *Computer Vision and Pattern Recognition*, pages 310–316, 2004.

[46] A. M. Buchanan and A. W. Fitzgibbon. Damped newton algorithms for matrix factorization with missing data. In *in CVPR05*, pages 316–322, 2005.

[47] S. Roweis. EM algorithms for pca and sensible pca. In *Neural Information Processing Systems*, 1997.

[48] T. Okatani and K. Deguchi. On the wiberg algorithm for matrix factorization in the presence of missing components. *Int. J. Comput. Vision*, 72:329–337, May 2007.

[49] K. Zhao and Z. Zhang. Successively alternate least square for low-rank matrix factorization with bounded missing data. *Comput. Vis. Image Underst.*, 114:1084–1096, October 2010.

[50] G. Lerman and T. Zhang. Robust recovery of multiple subspaces by geometric ℓ_p minimization. To appear in Annals of Statistics. Available at http://arxiv.org/abs/1104.3770.

[51] G. Liu, Z. Lin, and Y. Yu. Robust subspace segmentation by low-rank representation. In *ICML*, 2010.

[52] G. Liu, Z. Lin, S. Yan, J. Sun, Y. Yu, and Y. Ma. Robust recovery of subspace structures by low-rank representation. Available at `http://arxiv.org/abs/1010.2955`.

[53] J. B. Tenenbaum, V. de Silva, and J. C. Langford. A global geometric framework for nonlinear dimensionality reduction. *Science*, 290(5500):2319–2323, 2000.

[54] S. Roweis and L. Saul. Nonlinear dimensionality reduction by locally linear embedding. *Science*, 290(5500):2323–2326, 2000.

[55] J. A. Lee and M. Verleysen. *Nonlinear Dimensionality Reduction*. Information Science and Statistics. Springer, 2007.

[56] R. R. Coifman and D. L. Donoho. Translation-invariant de-noising. In *Wavelets and Statistics*, pages 125–150. Springer-Verlag, 1995.

[57] L. Bottou and Y. Bengio. Convergence properties of the k-means algorithms. In *Advances in Neural Information Processing Systems 7*, pages 585–592. MIT Press, 1995.

[58] J. Tropp, I. Dhillon, R. Heath, and T. Strohmer. Designing structured tight frames via alternating projection. *IEEE Trans. Inform. Theory*, pages 188–209, 2003.

[59] L. Balzano, B. Recht, and R. Nowak. High-dimensional matched subspace detection when data are missing. In *Proceedings of the International Symposium on Information Theory*, June 2010.

[60] W. I. Zangwill. *Nonlinear Programming: A Unified Approach.* Engle-wood Cliffs, NJ: Prentice-Hall, 1969.

[61] R. R. Meyer. Sufficient conditions for the convergence of monotonic mathematical programming algorithms. *J. Comput. System Sci.*, 12:108–121, 1976.

[62] G. B. Dantzig, J.Folkman, and N. Shapiro. On the continuity of the minimum set of continuous functions. *J. Math. Anal. Appl.*, 17:519–548, 1967.

[63] J. C. Fiorot and P. Huard. Composition and union of general algorithms of optimization. *Point-to-Set Maps and Mathematical Programming, Mathematical Programming Studies*, 10:69–85, 1979.

[64] D. Martin, C. Fowlkes, D. Tal, and J. Malik. A database of human segmented natural images and its application to evaluating segmentation algorithms and measuring ecological statistics. In *ICCV*, volume 2, pages 416–423, July 2001.

[65] M. Aharon, M. Elad, and A. Bruckstein. k -svd: An algorithm for designing overcomplete dictionaries for sparse representation. *Signal Processing, IEEE Transactions on*, 54(11):4311 –4322, 2006.

[66] A. Buades, B. Coll, and J. Morel. A non-local algorithm for image denoising. In *Computer Vision and Pattern Recognition*, pages 60–65, 2005.

[67] G. Peyre. Toolbox non-local means, Jun. 2009. `http://www.mathworks.com/matlabcentral /fileexchange/13619`.

[68] Z. Wang, A. C. Bovik, H. R. Sheikh, and E. P. Simoncelli. Image quality assessment: From error visibility to structural similarity. *IEEE Trans. Image Process.*, 13(4):600–612, 2004.

[69] M. B. Wakin. Manifold-based signal recovery and parameter estimation from compressive measurements. Technical report, 2008.